
Article:
Egan, J.E., Feng, W., James, A.D. et al. (Accepted: 2026) Ferric chloride: the Venusian unknown UV absorber? Journal of Geophysical Research: Planets. ISSN: 2169-9097 (In Press)

Journal of Geophysical Research: Planets

Ferric chloride: the Venusian unknown UV absorber?

Joanna V. Egan[1] (0000-0001-9676-3990, jo.egan@open.ac.uk); Wuhu Feng[1,2] (0000-0002-9907-9120); Alexander D. James[1] (0000-0003-0532-0065); James Manners[3] (0000-0003-4402-6811); Daniel R. Marsh[1,4] (0000-0001-6699-494X); Sébastien Lebonnois[5] (0000-0002-2390-8164); Franck Lefèvre[6] (0000-0001-5294-5426); Aurélien Stolzenbach[7] (0000-0001-6169-6820); John M. C. Plane[1] (0000-0003-3648-6893, j.m.c.plane@leeds.ac.uk)

[1] School of Chemistry, University of Leeds, Leeds, UK; [2] NCAS, University of Leeds, Leeds, UK; [3] Met Office, Fitzroy Road, Exeter, UK; [4] School of Physics and Astronomy, University of Leeds, Leeds, UK; [5] Laboratoire de Météorologie Dynamique, Sorbonne Université, ENS, PSL Research University, École Polytechnique, Institut Polytechnique de Paris, CNRS, Paris, France; [6] LATMOS, Sorbonne Université, UVSQ Paris-Saclay, CNRS, Paris, France; [7] Instituto de Astrofisica de Andalucia (IAA/CSIC), Granada, Spain

Key points

- ~1 wt% $FeCl_3$ in the Venusian clouds can reproduce the observed near-UV absorption, consistent with descent probe measurements.
- $FeCl_3$ can be produced from Fe ablated from cosmic dust above 100 km, and atmospheric HCl and Cl.
- The best fit to observations occurs when $FeCl_3$ is mostly present in mode 1 cloud droplets.

Abstract

Near-ultraviolet imaging of the planet Venus reveals inhomogeneous absorption features in the otherwise bright clouds. This absorption has been studied for nearly 100 years, but identification of the near-UV absorber remains one of the largest open questions in Venusian research. Based on a multiple scattering radiative transfer model, the observed absorption between 300 and 600 nm can be produced by 1.0 – 1.2 wt% ferric chloride ($FeCl_3$) in the mode 1 (~0.2 µm radius) sulfuric acid cloud droplets – less than the in-cloud iron mass loading measured during the Venera-12 mission. We present a novel chemical network within a global chemistry-climate model, which provides the required source of $FeCl_3$ in the upper cloud region from the reaction of Fe-containing molecules, produced by the ablation of cosmic dust particles, with atmospheric HCl. A residence lifetime of ~3000 years is required to provide sufficient optical absorption from a purely meteoric source of $FeCl_3$.

Plain language summary

Iron chloride has been proposed to cause the strong absorption seen in Venus's clouds. Using computer modeling of light in the atmosphere, we test the effect of iron chloride in the droplets that make up the Venusian clouds. We find that a modest concentration of 1.0 – 1.2 % (by mass) in the smallest cloud droplets can reproduce the shape and strength of the absorption recorded by the MESSENGER spacecraft. We present chemical reactions that produce iron chloride from the reaction of atmospheric hydrochloric acid gas and iron atoms produced from vapourised cosmic dust, and estimate that the iron chloride would take approximately 3000 years to concentrate enough to match observations of the clouds.

Index terms and keywords

6295 Venus; 5405 Atmospheres; 3337 Global Climate Models; 3359 Radiative Processes; 0317 Chemical Kinetics and photochemical properties

Venus; unknown UV absorber; FeCl3; meteoric material, atmospheric modelling

1. Introduction

The Venusian cloud deck is known to consist of a persistent multimodal system of cloud droplets, composed predominantly of concentrated sulfuric acid (Esposito et al., 1983; Knollenberg & Hunten, 1980; Titov et al., 2018). Sulfuric acid is bright when viewed at near-ultraviolet (NUV) wavelengths; however, spectra and images of the cloud tops show strongly-absorbing regions, spanning wavelengths between 300 – 600 nm, at most latitudes (e.g. Crisp, 1986; Lee et al., 2022; Pérez-Hoyos et al., 2018; Ross, 1928; Rossow et al., 1980; Wright, 1927). Many sulfur-containing candidates have been proposed to account for the NUV absorption, including polysulfur (Francés-Monerris et al., 2022; Hapke &

Graham, 1989; Pinto et al., 2021), polysulfur oxide (Hapke & Graham, 1989; Pinto et al., 2021), and iron-sulfur minerals (Jiang et al., 2024), but none have been conclusively identified as the cause of the absorption. The identification of the "unknown UV absorber" remains one of the largest open questions in Venusian atmospheric research (Crisp, 1986; Titov et al., 2018).

Ferric chloride ($FeCl_3$) has also been proposed as a candidate for the unknown absorber (Krasnopolsky, 2017; Kuiper, 1969; Zasova et al., 1981). Zasova et al. (1981) suggested that 1 wt% $FeCl_3$ in the mode 2 (~1 µm radius) sulfuric acid cloud droplets would satisfactorily match the observed planetary albedo, but did not provide their reference spectrum of $FeCl_3$. Comparisons of the relative agreement of different absorber candidates with measured spectra therefore used an absorption spectrum of $FeCl_3$ which was not measured under Venusian conditions (Aoshima et al., 2013; Pérez-Hoyos et al., 2018), and gave poor agreement with the Venusian spectrum, leading to the rejection of $FeCl_3$ as a candidate compared to other species. While some proposed candidates for the absorber have similar spectral shapes, none have yet been able to reproduce the precise spectrum of the NUV absorption at reasonably achievable atmospheric concentrations (e.g. Egan et al., 2025a; Jiang et al., 2024; Lefèvre et al., 2026; Pérez-Hoyos et al., 2018; Pinto et al., 2021; Skog et al., 2024). A recent measurement of the absorption spectrum of $FeCl_3$ in sulfuric acid (Egan et al., 2025b) showed much improved agreement of the $FeCl_3$ spectrum to that of the unknown absorber, compared with previous $FeCl_3$ spectra available in the literature. Furthermore, re-analysis of data from the Pioneer Venus Large Probe Gas Chromatograph (Mogul et al., 2025) revealed high concentrations of iron in the clouds, similar to reported X-ray fluorescence measurements of iron from Venera 12 (Petryanov et al., 1981). In light of the combination of observed high iron concentrations and the availability of a more applicable $FeCl_3$ spectrum, the suitability of $FeCl_3$ to provide significant NUV absorption should be reconsidered.

Here we investigate whether there is a feasible source of Fe from meteoric ablation, and chemical pathways to produce enough $FeCl_3$ in the upper clouds, to reproduce the observed NUV features in the reflectance spectrum of Venus. The possibility of a meteoric component to the NUV absorber has been suggested in the past (Knollenberg & Hunten, 1979; Pollack et al., 1979), though small fragments of meteoric material were considered, rather than the products of ablated (i.e. vaporized) elements. In addition, the role of meteoric material was recently investigated by Karyu et al. (2026), who found that ablated cosmic dust particles drive the formation of the lower haze, and can act as condensation nuclei for the main cloud deck. Studies of the atmospheres of Earth and Mars (Carrillo-Sánchez et al., 2020; Crismani et al., 2017; Gómez Martín et al., 2017; Grebowsky et al., 2017; Plane, 2003a; Plane et al., 2018a; Plane et al., 2015) have shown that the ablation of cosmic dust particles from comets and asteroids injects a variety of metals (Fe, Mg, Na, etc.) into the atmospheres of the terrestrial planets. The Fe meteoric input function for Venus has been estimated using an astronomical dust model

coupled to a chemical ablation model (Carrillo-Sánchez et al., 2020). Here we then model the production of $FeCl_3$ from the reaction of meteoric Fe-containing molecules (primarily carbonates) and chlorine-containing species (HCl, Cl) of presumably volcanic origin, using a new chemical network implemented in the Venus Planetary Climate Model (V-PCM) (Gilli et al., 2021; Martinez et al., 2024; Martinez et al., 2023; Stolzenbach et al., 2023). The required concentration of $FeCl_3$ to reproduce the observed top-of-atmosphere (TOA) reflectance is estimated using the multiple scattering radiative transfer model SOCRATES (Egan et al., 2025a; Manners et al., 2022a, 2022b), from which the residence lifetime of $FeCl_3$ in the upper clouds can be estimated.

2. Modelling

Two modelling approaches are used in this study: the chemical network for the formation of gas phase $FeCl_3$ from meteoric Fe was studied using a 3D global climate model (Section 2.1). A separate 1D radiative transfer model (Section 2.2) was run to predict the required $FeCl_3$ concentration in the clouds to reproduce observations.

2.1 Photochemical modelling

3D photochemical modelling was performed using the V-PCM (e.g., Garate-Lopez & Lebonnois, 2018; Martinez et al., 2024; Martinez et al., 2023; Stolzenbach et al., 2023), version r3188. A horizontal grid size of 1.875° × 3.75° was used, with 90 pressure levels from the surface to 8×10^{-9} Pa, ~250 km, resulting in model layers of 2 – 3 km thickness through the clouds. The model was initialised with steady-state conditions from the Venus Climate Database v2.3 (Martinez et al., 2024), available at http://www-venus.lmd.jussieu.fr/). For illustrative purposes, the equatorial mean of the initial temperature, vertical diffusion coefficient, and mixing ratios of relevant species are shown in Figure S1 (Supplemental Information, SI). The model was run for 3.0 Venus solar days (Vd).

The ablation of meteoric material in the atmosphere provides a flux of many metals, including iron, into the upper atmosphere. The ablated Fe injection rate of 4.09 t d^{-1} from Carrillo-Sánchez et al. (2020) was adopted, with 72% injected as Fe and the remainder as Fe^+. Note that the evaporating Fe atoms initially have essentially the same velocity as the parent meteoroid from which they ablate. The first (hyperthermal) collision with the main atmospheric constituent (CO_2) can then lead to ionization with a probability that increases with increasing velocity (Janches et al., 2017), and also reaction to produce FeO + CO (as investigated previously for the ablation of Mg (Plane et al., 2018b)). FeO will be quickly reduced to Fe by reaction with O or CO (Table 1). Further collisions with CO_2 of any surviving translationally hot Fe atoms will rapidly quench them (within typically 10 collisions) to the temperature of the background atmosphere, so that further chemistry will involve thermal reactions.

The Fe chemistry network added to the V-PCM is shown in Table 1 and Figure 1. Novel reactions, which have not been included previously in models of Fe in the upper atmospheres of Earth (Feng et al., 2013) or Mars (Whalley & Plane, 2010), are identified by footnote 5 in Table 1. The rate coefficients for these reactions were calculated using electronic structure (ab initio quantum) theory combined with statistical rate theories (Frisch et al., 2016; Georgievskii & Klippenstein, 2005; Gilbert & Smith, 1990; Glowacki et al., 2012; Montgomery et al., 2000; Scalmani et al., 2006; Smith, 1980; Tobiska et al., 2000), described in detail in the SI. For ease of reproduction, both the full polynomial forms of the reaction coefficients for reactions 5 and 9 and a simplified Kooij form that may be more readily implemented in other photochemical models are provided. The calculation of the photolytic rate coefficients and the photodissociation threshold wavelengths for each photochemically active species are also described in the SI.

We have extensively used these theoretical methods of rate coefficient calculation to fit measured rate coefficients for reactions of both neutral and ionized metal atoms, oxides and hydroxides with atmospheric species, reactions which often occur over multi-well potential energy surfaces (e.g. Bones et al., 2020; Gómez-Martín et al., 2017; Mangan et al., 2020; Plane, 2003b). While this experience means that we expect a rate coefficient estimated purely theoretically to be uncertain perhaps within a factor of 2, the important first step is to establish whether the reaction is likely to be important at low temperatures (< 300 K in the case of Venus's upper atmosphere). This means that the overall reaction should be exothermic and that any barriers between local minima are submerged with respect to the entrance channel. Global mean mixing ratios of key iron species after three Venus solar days are shown in Figure 2. Profiles of all iron species are shown in Figure S2 (SI). Cross-sections of photolytically active species are shown in Figure S5 (SI).

Table 1. Fe chemistry network in the V-PCM.

No.	Reaction	Rate Coefficient[a]	Note
		Neutral reactions	
1	$Fe + O_3 \rightarrow FeO + O_2$	$3.4 \times 10^{-10} \exp(-146/T)$	1
2	$FeO + O \rightarrow Fe + O_2$	$4.6 \times 10^{-10} \exp(-350/T)$	2
3	$FeO + CO \rightarrow Fe + CO_2$	$1.2 \times 10^{-13}(T/300)^{2.307} \exp(-820/T)$	3
4	$FeO + O_3 \rightarrow FeO_2 + O_2$	$3.0 \times 10^{-10} \exp(-177/T)$	4
5	$FeO + CO_2 (+ M) \rightarrow FeCO_3$	$\log_{10}(k_{rec,0}) = \log_{10}(2)$ $- 37.87+7.074\log_{10}T-1.649(\log_{10}T)^2$ or $2.67 \times 10^{-30}(T/300)^{-2.53} \exp(-410/T)$	4
6	$FeO_2 + O \rightarrow FeO + O_2$	$1.4 \times 10^{-10} \exp(-580/T)$	2
7	$FeO_2 + CO_2 (+M) \rightarrow OFeCO_3$	$1.3 \times 10^{-30} (T/300)^{-4.06}$	5
8	$OFeCO_3 + O \rightarrow FeCO_3 + O_2$	$2.0 \times 10^{-10} (T/300)^{0.167}$	5
9	$FeCO_3 + CO_2 (+M) \rightarrow FeCO_3.CO_2$	$\log_{10}(k_{rec,0}) = \log_{10}(2) - 51.8343$ $+ 26.43\log_{10}T - 6.335(\log_{10}T)^2$ or $5.78 \times 10^{-24}(T/300)^{-8.67} \exp(-1173/T)$	5
10	$FeCO_3.CO_2 + O \rightarrow OFeCO_3 + CO_2$	$2.0 \times 10^{-10} (T/200)^{0.167}$	5
11	$FeCO_3.CO_2 (+M) \rightarrow FeCO_3 + CO_2$	$k_9/(6.78 \times 10^{-25} \exp(13387/T))$	5
12	$FeCO_3 + HCl \rightarrow HOFeCl + CO_2$	$2.0 \times 10^{-10} (T/200)^{0.167}$	5
13	$FeCO_3.CO_2 + HCl \rightarrow HOFeCl + 2CO_2$	$2.0 \times 10^{-10} (T/200)^{0.167}$	5
14	$HOFeCl + HCl \rightarrow FeCl_2 + H_2O$	$2.0 \times 10^{-10} (T/200)^{0.167}$	5
15	$FeCO_3 + Cl \rightarrow OFeCl + CO_2$	$2.0 \times 10^{-10} (T/200)^{0.167}$	5
16	$FeCO_3.CO_2 + Cl \rightarrow OFeCl + 2CO_2$	$2.0 \times 10^{-10} (T/200)^{0.167}$	5
17	$OFeCl + Cl \rightarrow FeCl_2 + O$	$2.0 \times 10^{-10} (T/200)^{0.167}$	5
18	$FeCl + O_3 \rightarrow OFeCl + O_2$	$2.0 \times 10^{-10} (T/200)^{0.167}$	5
19	$FeCl_2.H_2O + Cl \rightarrow FeCl_3 + H_2O$	$2.0 \times 10^{-10} (T/200)^{0.167}$	5
20	$FeCl_2 + H_2O (+ M) \rightarrow FeCl_2.H_2O$	$8.6 \times 10^{-26} (T/200)^{-5.06}$	5
21	$FeCl_3 + CO_2 (+M) \rightarrow FeCl_3.CO_2$	$1.2 \times 10^{-28} (T/200)^{-6.53}$	5
22	$FeCl_3.CO_2 (+M) \rightarrow FeCl_3 + CO_2$	$5.1 \times 10^{-8} \exp(-3012/T)$	5
		Ion-molecule reactions	
23	$Fe^+ + O_3 \rightarrow FeO^+ + O_2$	$7.1 \times 10^{-10} \exp(-129/T)$	6
24	$FeO^+ + O \rightarrow Fe^+ + O_2$	3.2×10^{-11}	7
25	$FeO^+ + CO \rightarrow Fe^+ + CO_2$	1.6×10^{-10}	7
26	$FeO^+ + CO_2 (+M) \rightarrow FeO^+.CO_2$	$3.2 \times 10^{-27} (T/300)^{-3.11}$	5
27	$Fe^+ + CO_2 (+M) \rightarrow Fe^+.CO_2$	$8.1 \times 10^{-29} (T/300)^{-2.31}$	8
28	$Fe^+.CO_2 + CO_2 (+M) \rightarrow Fe^+.(CO_2)_2$	$4.6 \times 10^{-28} (T/300)^{-5.38}$	5
29	$Fe^+.CO_2 + O \rightarrow FeO^+ + CO_2$	4.6×10^{-10}	5
30	$Fe^+.(CO_2)_2 + O \rightarrow FeO^+.CO_2 + CO_2$	5.0×10^{-10}	5
31	$FeO^+.CO_2 + CO_2 (+M) \rightarrow FeO^+.(CO_2)_2$	$2.3 \times 10^{-26} (T/300)^{-5.52}$	5

32	$FeO^+.CO_2 + O \rightarrow FeO_2^+ + CO_2$	$7.0 \times 10^{-11} (T/300)^{-0.33}$	5
33	$FeO^+.CO_2 + O \rightarrow Fe^+.CO_2 + O_2$	$3.1 \times 10^{-10} (T/300)^{0.03}$	5
34	$FeO_2^+ + O \rightarrow FeO^+ + O_2$	6.3×10^{-11}	7
35	$FeO^+ + e^- \rightarrow Fe + O$	$5.5 \times 10^{-7} (T/300)^{-0.5}$	9
36	$FeO_2^+ + e^- \rightarrow Fe + O_2$	$5.5 \times 10^{-7} (T/300)^{-0.5}$	10
37	$Fe^+.CO_2 + e^- \rightarrow Fe + CO_2$	$5.5 \times 10^{-7} (T/300)^{-0.5}$	10
38	$Fe^+.(CO_2)_2 + e^- \rightarrow Fe + CO_2 + CO_2$	$5.5 \times 10^{-7} (T/300)^{-0.5}$	10
39	$FeO^+.CO_2 + e^- \rightarrow FeO + CO_2$	$5.5 \times 10^{-7} (T/300)^{-0.5}$	10
40	$FeO^+.(CO_2)_2 + e^- \rightarrow FeCO_3 + CO_2$	$5.5 \times 10^{-7} (T/300)^{-0.5}$	10
41	$FeO_2^+.CO_2 + e^- \rightarrow FeO_2 + CO_2$	$5.5 \times 10^{-7} (T/300)^{-0.5}$	10
42	$FeO^+.(CO_2)_2 + O \rightarrow FeO_2^+.CO_2 + CO_2$	$3.1 \times 10^{-10} (T/300)^{0.03}$	5
43	$Fe + O_2^+ \rightarrow Fe^+ + O_2$	1.1×10^{-9}	11
44	$Fe + NO^+ \rightarrow Fe^+ + NO$	9.2×10^{-10}	11
45	$FeCO_3 + O_2^+ \rightarrow FeO^+.CO_2 + O_2$	1.0×10^{-9}	12
46	$FeCO_3 + NO^+ \rightarrow FeO^+.CO_2 + NO$	1.0×10^{-9}	12
47	$FeCO_3.CO_2 + O_2^+ \rightarrow FeO^+.(CO_2)_2 + O_2$	1.0×10^{-9}	12
48	$FeCO_3.CO_2 + NO^+ \rightarrow FeO^+.(CO_2)_2 + NO$	1.0×10^{-9}	12
49	$Fe^+ + e^- \rightarrow Fe + h\nu$	$6.5 \times 10^{-12} (T/300)^{-0.51}$	13
Photochemical reactions			
50	$Fe + h\nu \rightarrow Fe^+ + e^-$	3.2×10^{-6}	14
51	$FeCl + h\nu \rightarrow Fe + Cl$	0.15	5
52	$FeCl_2 + h\nu \rightarrow FeCl + Cl$	2.0×10^{-3}	5
53	$FeCl_3 + h\nu \rightarrow FeCl_2 + Cl$	2.3×10^{-2}	5
54	$FeCO_3 + h\nu \rightarrow FeO + CO_2$	0.17	5
55	$FeCl_3.CO_2 + h\nu \rightarrow FeCl_3 + CO_2$	0.41	5
56	$FeCO_3.CO_2 + h\nu \rightarrow FeO + 2CO_2$	0.20	5
57	$OFeCO_3 + h\nu \rightarrow FeO_2 + CO_2$	0.34	5

[a] Units: photolysis reactions, s^{-1}; bimolecular reactions, cm^3 $molecule^{-1}$ s^{-1}; termolecular, cm^6 $molecule^{-2}$ s^{-1}. 1.Helmer and Plane (1994). 2.Self and Plane (2003). 3. A best fit using Transition State Theory to the literature rate coefficients for the reverse reaction, $Fe + CO_2 \rightarrow FeO + CO$ (Giesen et al., 2002; Smirnov, 2008). 4. Rollason and Plane (2000). 5. This work (see text and SI). 6. Rollason and Plane (1998). 7. Woodcock et al. (2006). 8. Vondrak et al. (2006). 9. Bones et al. (2016). 10. Set to the measured rate coefficient for $FeO^+ + e^-$ (Bones et al., 2016). 11. Rutherford and Vroom (1972). 12. Set to a typical charge transfer rate coefficient cf. reactions 43 and 44. 13. Nahar et al. (1997). 14. Whalley and Plane (2010), rescaled for Venus.

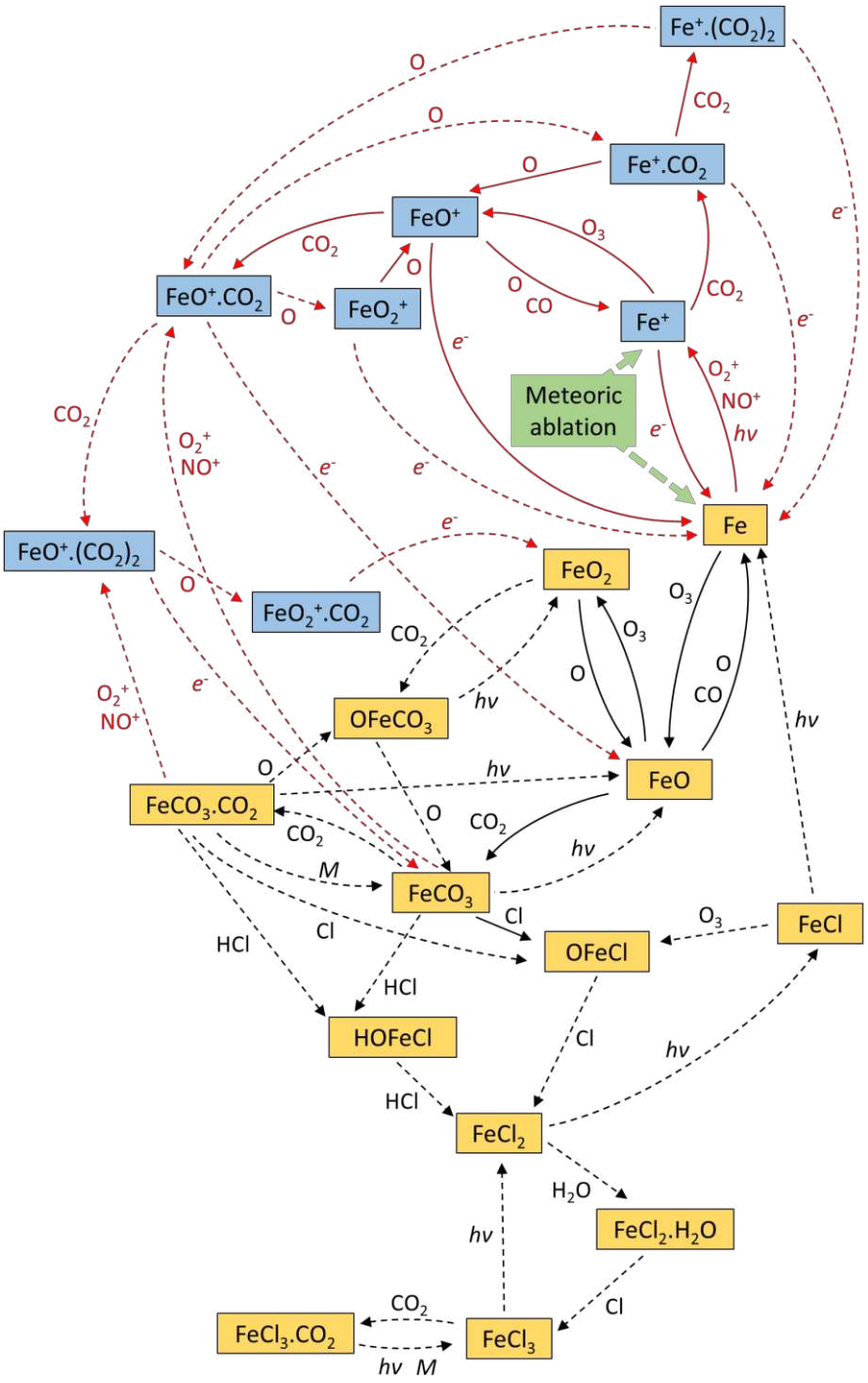

Figure 1. Chemical network of 57 Fe-species reactions implemented in the V-PCM (see Table 1 for reaction rate coefficients). Neutral and ionized species are shown in gold and blue boxes, respectively. Ion-molecule reactions (red) and neutral reactions (black) that have been measured experimentally are indicated with solid arrows, predicted rates are shown with dashed arrows. hν indicates photolysis or photoionisation, e^- are electrons, and M is a third body (usually CO_2).

The V-PCM cloud treatment, described in Stolzenbach et al. (2023) distributes the calculated liquid phase from the microphysical cloud model to the cloud modes according to the mass loading of the Venus standard cloud model (Knollenberg & Hunten, 1980), derived from the Pioneer Venus Large Probe Cloud Particle Size Spectrometer (LCPS) measurements. All modes are described with log-normal distributions. The values used for these cloud modes are listed in Table S4 (SI). The condensed mass of H_2O and H_2SO_4 calculated by the V-PCM and adopted for use in SOCRATES is shown in Figure S6 (SI).

2.2 Radiative transfer modelling

1D multiple scattering radiative transfer modelling was performed using SOCRATES (Manners et al., 2022a, 2022b). A two-stream approximation is used to resolve the upward and downward direct and diffuse fluxes through the atmosphere (Edwards & Slingo, 1996). Before the two-stream equations can be formed and solved, the gas absorption coefficients are determined, and a spectral file produced. The correlated-k method (Goody et al., 1989) is used to treat the absorption. SOCRATES was developed to model the Earth's atmosphere, but has been adapted for Venus (Egan et al., 2025a). The atmosphere is modeled with 5 nm bands from 175 – 700 nm. Temperature, pressure, cloud modes, and gas abundances (except SO_2) from the V-PCM are adopted wherever possible, or taken from Eymet et al. (2009) for species that are not included in the V-PCM (HF, H_2S, and the HDO:H_2O ratio). The V-PCM is unable to reproduce the observed decrease in SO_2 through the clouds (a significant unsolved issue in all Venus models (Vandaele et al., 2017)), so a constructed SO_2 profile, in line with observations, was adopted instead (see figure S7, SI). Gas absorption coefficients from Gordon et al. (2022) and the refractive indices for sulfuric acid from Palmer and Williams (1975) were used.

The effect of the inclusion of $FeCl_3$ in each cloud mode was modelled using the $FeCl_3$ spectra measured by Egan et al. (2025b). Spectra measured for sample x0C (1.72(3) M $FeCl_3$ in 76.7(5) wt% sulfuric acid, with an initial HCl concentration of 9.2(3) × 10^{-3} M, see that paper for further details) were used in all cases. SOCRATES employs Mie theory to calculate the aerosol extinction for each cloud mode. The measured molar absorptivity, ε (units: L mol^{-1} m^{-1}), was converted to imaginary refractive index, k, using

$$k = \frac{\varepsilon c \lambda_0}{4\pi \log_{10}(e)} \quad (1)$$

where c is the concentration of Fe (in mol dm^{-3}) in the solution and λ_0 is the vacuum wavelength of light (in m). The real refractive index was held constant for all concentrations of Fe, and the imaginary refractive index was taken to be that of pure sulfuric acid beyond 600 nm. Spectra were compared to MASCS/MESSENGER reflectance spectrum 151 (Pérez-Hoyos et al., 2018).

Figure 3 shows the effect of the progress of the reaction (i.e., the ratio of ferric chloride to ferric sulfate ions) on the shape of the absorption, which was considered by adopting spectra measured on days 1, 4, 9, and 18 in Egan et al. (2025b) (from their Figure S1b). Samples consisting of 70:30% ferric chloride:ferric sulfate ions (measured on day 4 of reaction progress) provided the best spectral fit to observations. Tests of $FeCl_3$ concentrations in different cloud modes found that $FeCl_3$ in all modes, or mode 1 only, provided the best fit to observations (Figures 3 and 4), so further consideration was limited to mode 1 only.

2.3 Residence lifetime calculation

The meteoric flux of iron into the Venusian atmosphere is 31 ± 18 t d^{-1}, of which approximately 13% (4.1 t d^{-1}) ablates (vaporizes) (Carrillo-Sánchez et al., 2020), becoming available for conversion to $FeCl_3$.

The required $FeCl_3$ atmospheric dynamical residence time (i.e. ignoring chemical removal of $FeCl_3$), $\tau_{\mathrm{FeCl_3}}$, for a purely meteoric source of iron in the upper clouds is estimated by

$$\tau_{\mathrm{FeCl_3}} = \frac{\varsigma_{\mathrm{FeCl_3}}}{\Phi_{m,\mathrm{FeCl_3}}} \tag{2}$$

where $\varsigma_{\mathrm{FeCl_3}}$ is the required $FeCl_3$ column mass density, and $\Phi_{m,\mathrm{FeCl_3}}$ is the meteoric mass flux of $FeCl_3$. The radiative transfer model was found to be sensitive only to the $FeCl_3$ concentration in the upper clouds (see Section 3.3), so only the required column mass density above 60 km is considered in this calculation. In this region, sedimentation of mode 1 particles is slow compared to the upwelling timescale (Stolzenbach et al., 2023). We therefore assume that sedimentation can be neglected in this calculation.

The $FeCl_3$ column mass density is calculated from the column mass density of mode 1, ς_1, found from the V-PCM cloud model (Figure S6, SI) to be 231 µg cm^{-2} above 60 km, and the best fit $FeCl_3$ wt% in the mode 1 droplets, denoted $w_{\mathrm{FeCl_3}}$:

$$\varsigma_{\mathrm{FeCl_3}} = w_{\mathrm{FeCl_3}}\varsigma_1 \tag{3}$$

The molar iron flux, $\Phi_{n,Fe}$, at the height of injection of iron h in the atmosphere is given by

$$\Phi_{n,\mathrm{Fe}} = \frac{\dot{m}_{\mathrm{Fe}}}{4\pi\,(R+h)^2\,M_{\mathrm{Fe}}} \tag{4}$$

where $\dot{m}_{\mathrm{Fe}}$ is the meteoric mass injection rate of ablated Fe, R is the radius of Venus and $M_{\mathrm{Fe}}$is the molar mass of iron. Assuming the upper limit of complete conversion of meteoric iron to $FeCl_3$, which remains in mode 1, $\Phi_{n,\mathrm{Fe}} = \Phi_{n,\mathrm{FeCl_3}}$, and the mass flux of $FeCl_3$ can be calculated using the molar mass of $FeCl_3$, $M_{\mathrm{FeCl_3}}$:

$$\Phi_{m,\mathrm{FeCl_3}} = \frac{\dot{m}_{\mathrm{Fe}} M_{\mathrm{FeCl_3}}}{4\pi\,(R+h)^2\,M_{\mathrm{Fe}}} \quad (5)$$

which can be substituted, along with Equation 3, into Equation 2:

$$\tau_{\mathrm{FeCl_3}} = \frac{4\pi(R+h)^2 M_{\mathrm{Fe}} w_{\mathrm{FeCl_3}} \varsigma_1}{\dot{m}_{\mathrm{Fe}} M_{\mathrm{FeCl_3}}} \quad (6)$$

3. Results

3.1 Distribution of iron-containing species

A chemical network (Figure 1) for the production of iron oxide, carbonate, and chloride species from ablated Fe in the Venusian upper atmosphere was developed (see Methods section, which lists the rate coefficients and method of theoretical calculation for reactions where rate coefficients have not been measured), and then implemented in the V-PCM. The initial source of iron into the model is provided by a global flux of 4.2 tonnes per Earth day of Fe (72%) and Fe^+ (28%), injected from 95 – 250 km (maximum at 115 km) (Carrillo-Sánchez et al., 2020). The ablation is not directly modelled, and as such the Fe and Fe^+ are added directly into the gas phase in thermal equilibrium with the surrounding atmosphere. As discussed in Section 2.1, hot ablated atoms are rapidly quenched by collision with CO_2, so this simplification is valid. A plot of the injection profile is available in Figure S10 (SI).

Figure 2 shows the modeled mean mixing ratio profiles of key Fe-containing species after a 3.0 Venus Vd simulation. Profiles of all iron species are shown in Figure S2 (SI). Fe and Fe^+ are the dominant species above 100 km. Fe is converted via FeO to $FeCO_3$, which reacts with abundant HCl and Cl to form $FeCl_3$. $FeCl_3$, clustered with CO_2, then becomes the dominant iron-containing species below 100 km. The latitude-weighted global mean flux of $FeCl_3$ and other reservoir species ($FeCl_3.CO_2$ and $FeCl_2.H_2O$) after 3.0 Vd is -8.1 × 10^4 molecules cm^{-2} s^{-1} at the base of the ablation profile (95 km), which is 84% of the column-integrated iron injection rate (here, the negative sign indicates a downward flux by convention). Vertical transport slower than the formation rates above 90 km results in the accumulation of $FeCl_3$, $FeCl_3.CO_2$, and $FeCl_2.H_2O$ in the layers seen in Figure 2. $FeCl_3$ formation continues in this region from Fe transported below the base of the ablation before reacting (Figure 2) and other intermediate species (Figure S2, SI), leading to complete conversion to $FeCl_3$ and the other reservoir species by ~75 km. Note that, while the atmosphere above 100 km reaches steady state, $FeCl_3$ and $FeCl_3.CO_2$ concentrations below 100 km are still increasing with time after 3.0 Vd and should continue to do so beyond reasonably achievable model run lengths. At altitudes near the base of the ablation, downward advection occurs predominantly on the night side of the planet. At ~±40 – 70° latitude, vertical transport increases near 85 km, transporting $FeCl_3$ and precursors more rapidly downwards into the clouds once they reach this region. Condensation of these species, or their uptake to cloud

and haze droplets, and their subsequent sedimentation will likely increase the rate of downward transport of $FeCl_3$ to the dynamically stable, stratified upper cloud region.

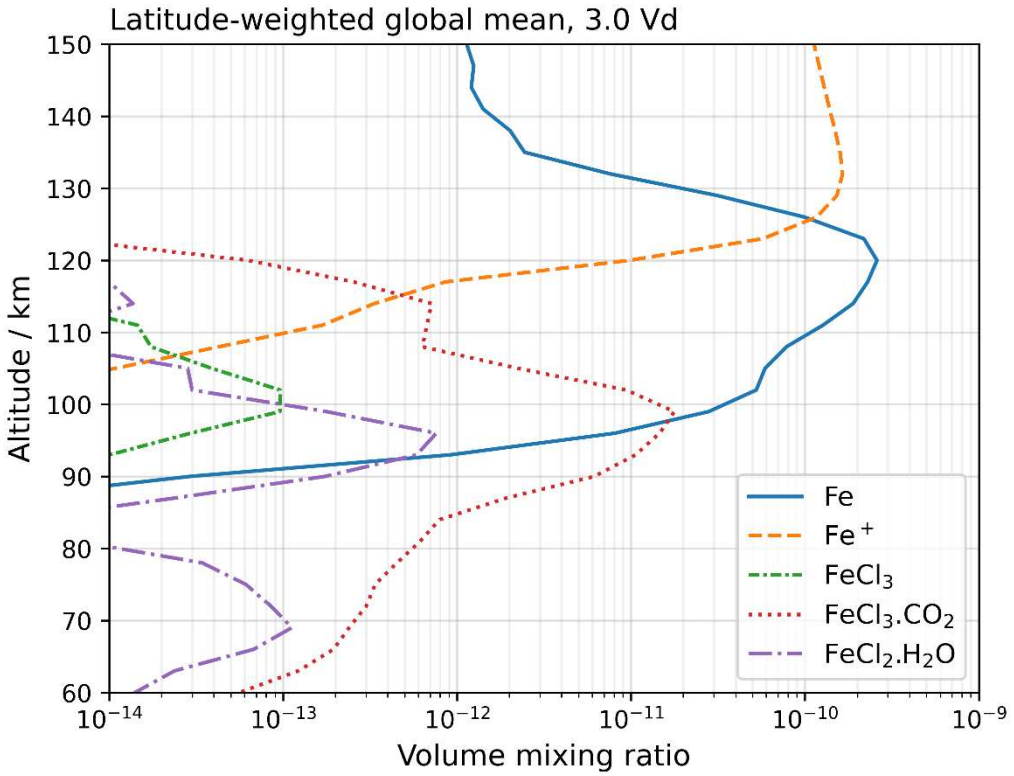

Figure 2. Latitude-weighted global mean mixing ratios of meteoric Fe and Fe^+ and $FeCl_3$ and reservoir species modelled in the V-PCM after 3.0 Vd. Concentrations of $FeCl_3$ will continue to build up over time. Note that the Fe species below 100 km are likely to begin to be taken up in haze or cloud droplets (Gao et al., 2014; Karyu et al., 2024; Luginin et al., 2024; Wilquet et al., 2012), rather than remaining solely in the gas phase.

3.2 Modelled reflectance

We assume that $FeCl_3$ and $FeCl_3.CO_2$, when taken up in Venusian cloud droplets, form solvated $FeCl_3$. Egan et al. (2025b) showed that ferric sulfate ions ($Fe(SO_4)_2^-$) form slowly from $FeCl_3$ in concentrated sulfuric acid (with a chemical lifetime of several weeks to over a year at 298 K), and that somewhat different Venusian spectra measured over time (Crisp, 1986; Lee et al., 2022; Pérez-Hoyos et al., 2018) could be reproduced by varying the ratio of ferric chloride to ferric sulfate. The most complete measured Venusian reflectance spectrum was obtained by the MASCS spectrometer on the spacecraft MESSENGER during its 2007 gravity assist manoeuvre at Venus (Pérez-Hoyos et al., 2018). The spectrum has good spectral resolution down to 300 nm, making it ideal for comparison in this work.

Initial tests were carried out using measured spectra from Egan et al. (2025b) with varying ratios of ferric chlorides to sulfates (Figure 3). The iron species were modelled as being present in the same

concentrations in all cloud modes. The best fit results are those with a 70:30% ferric chloride to sulfate ratio (Figure 3b), which satisfactorily reproduces the shape of the absorption well throughout the wavelength range. The variation in spectral shape at 500 – 600 nm is assumed to be due to the variation in chlorination of the iron ($FeCl_n^{3-n}$ ions) (Egan et al., 2025b; Liu et al., 2006), which causes variation in the precise shape of the absorption spectrum.

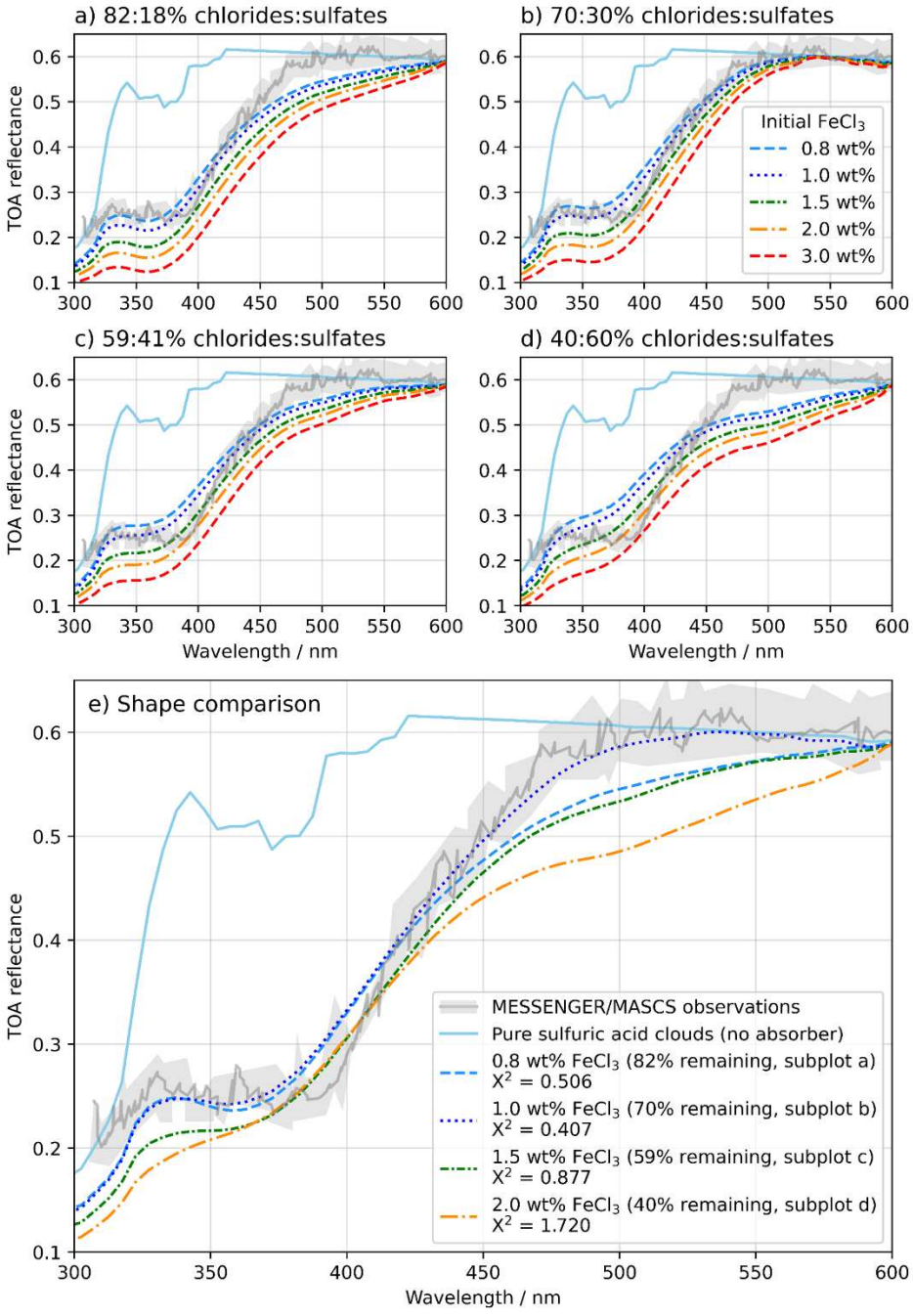

Figure 3. Best fit to MESSENGER observations (grey line and uncertainty region, Pérez-Hoyos et al., 2018) for different initial concentrations of $FeCl_3$ using spectra containing iron chloride:sulfate molar ratios of a) 82:18% b) 70:30%, c) 59:41%, d) 40:60%. The concentration in the legend refers to the

initial wt% of $FeCl_3$ in the sample, some fraction of which (given in subplot title) has reacted to form sulfates i.e., it is not the instantaneous ferric chloride concentration in the samples at the time the spectrum was measured. The predicted spectrum of Venus in the absence of any NUV absorber candidate (light blue line) is shown for comparison. The iron concentrations that provide the most similar value of reflectance near 365 nm are shown in subplot e to aid in comparison of shapes. The line colours are consistent in all the figure panels. The quality of the fit is calculated as $X^2 = \sum_\lambda \left(\frac{observation-model}{observation}\right)^2$, where the MESSENGER observations (grey line) have been interpolated to the wavelength (λ) values of the model.

3.3 Sensitivity of the reflected spectrum to cloud mode

The Venusian clouds are made up of different sizes of cloud droplets, divided into four size modes: ~0.2 µm radius "mode 1" droplets throughout the cloud deck; ~1.0 µm radius "mode 2" droplets in the upper and lower cloud layers, growing into a slightly larger ~1.4 µm radius "mode 2'" in the middle clouds; and 3.65 µm "mode 3" droplets in the middle and lower clouds (Knollenberg & Hunten, 1980; Stolzenbach et al., 2023; Tomasko et al., 1980). Sensitivity tests were carried out to predict the effect of $FeCl_3$ in the different Venusian cloud modes (Figure 4). The observed reflectance spectrum (Pérez-Hoyos et al., 2018) could be reproduced with $FeCl_3$ in all cloud modes (Figure 3b), or else exclusively in mode 1 (Figure 4). An initial concentration of ~10 wt% $FeCl_3$ in mode 2 was able to reproduce the strength of the absorption near 360 nm reasonably well, but the quality of the fit at long wavelengths is poor.

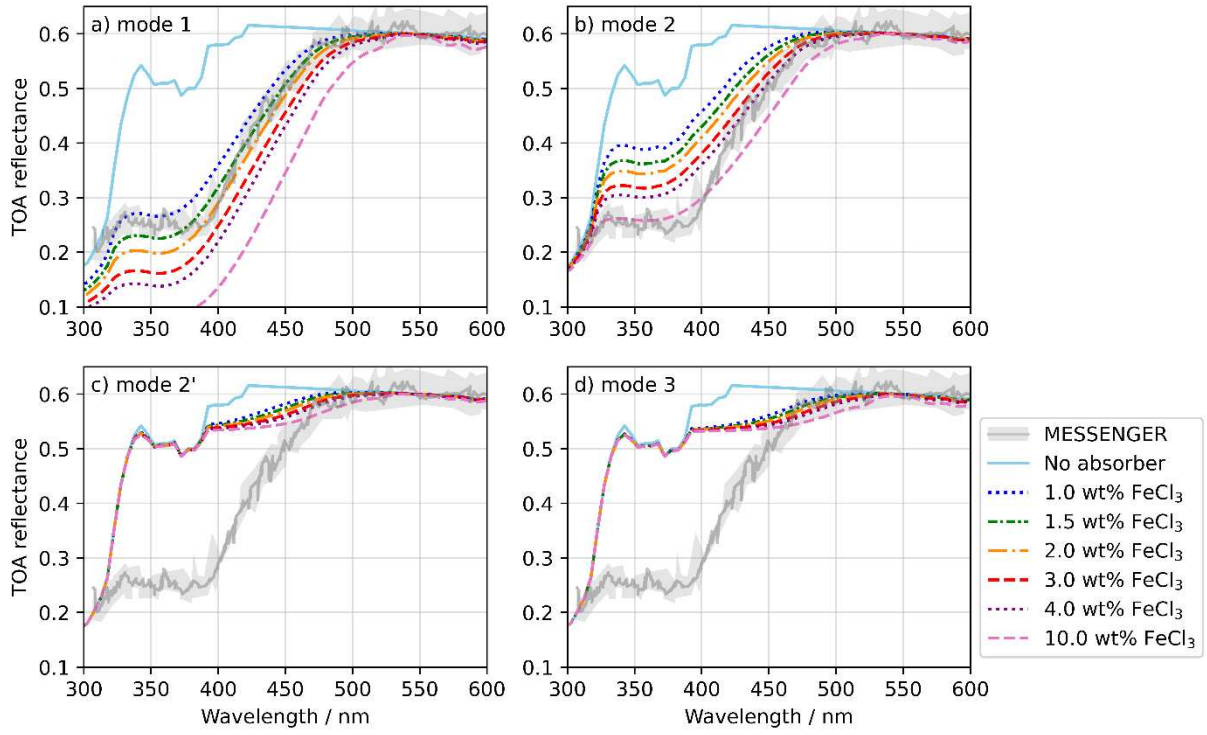

289 **Figure 4.** Comparison of the MESSENGER reflectance spectrum (grey line and uncertainty region,
290 Pérez-Hoyos et al., 2018) with the predicted spectrum in the absence of an absorber (light blue line)
291 and predicted spectra of different initial concentrations of $FeCl_3$ in a) mode 1 b) mode 2, c) mode 2',
292 and d) mode 3.

293 Even high concentrations (> 10 wt% $FeCl_3$) in modes 2' or 3 were not able to reproduce the observed
294 absorption. This is because both cloud modes are located too far below the cloud top to contribute a
295 significant amount of observable absorption. The model is not sensitive to their composition with this
296 cloud configuration, so no further conclusions can be drawn. Despite the sensitivity of the model to
297 mode 2 in the upper clouds, only mode 1 is considered henceforth due to its dominant effect. We
298 emphasise that the dominance of mode 1 does not preclude the presence of $FeCl_3$ in other cloud
299 modes, but it is not required to explain the absorption.

300 ### 3.4 Improvements to the spectral shape

301 The predicted absorption in Figure 4 is generally higher than observations near 300 nm when the rest
302 of the fit is good, which may indicate that the concentration of one or more of the absorbing species
303 ($FeCl_n^{3-n}$, $Fe(SO_4)_2^-$, SO_2) is over-estimated. Inspection of the wavelength regions of absorption due to
304 ferric chloride and ferric sulfate ions reported by Egan et al. (2025b) shows that ferric sulfate absorbs
305 at all wavelengths below 400 nm, with a peak around 290 nm and so would therefore contribute to
306 the modeled absorption near 300 nm. The dominant effect is due to SO_2 in this region, which has
307 historically been assumed to be the only absorbing species at these wavelengths (e.g. Crisp, 1986). The
308 reaction of ferric chloride to form ferric sulfate depends on the chloride concentrations of the solution
309 (Egan et al., 2025b), with high chloride concentrations shifting the reaction equilibrium to favour ferric
310 chloride, rather than ferric sulfate species. The high gas-phase HCl concentration in the Venusian
311 clouds (~0.1 – 0.4 ppm, Figure S8, SI; Bertaux et al., 2007; Bézard et al., 1990; Krasnopolsky, 2010a;
312 Mahieux et al., 2023b; Vandaele et al., 2008; Young, 1972) will maintain a higher Cl^- concentration in
313 the droplets (~10^{-3} – 10^{-4} M near 90 km (~170 K), decreasing to 10^{-5} M near 56 km (~300 K) (Figure S9,
314 SI; Williams & Golden, 1993) than was achievable in the laboratory work of Egan et al. (2025b) at 298
315 K and with unmeasurable but likely negligible HCl in the headspace above the samples. In addition,
316 the V-PCM temperature of 200 – 250 K in the upper cloud region, similar to observations (Ando et al.,
317 2020; Seiff et al., 1985; Tellmann et al., 2009) should slow the conversion of Fe chloride to sulfate by
318 reducing the reaction rate in addition to increasing HCl solubility in the droplets. Thus, higher ferric
319 chloride fractions are likely in the upper clouds, compared with the laboratory measurements.

320 Three cases are considered to examine the effect of sulfur-containing species near 300 nm: mode 1
321 contains some concentration of ferric chloride and ferric sulfate in a 70:30% ratio as measured in Egan

et al. (2025b) (Figure 5a); mode 1 contains some concentration of ferric chloride, and the formation of ferric sulfate is negligible in the optically relevant upper cloud region (Figure 5b); and mode 1 contains a 70:30 ratio of ferric chloride to ferric sulfate, but the atmospheric SO_2 mixing ratio throughout the atmosphere (~150 ppm below the cloud deck and 0.01 - 1 ppm above the clouds, Figure S7, SI; Belyaev et al., 2012; Bertaux et al., 1996; Bézard et al., 1993; Encrenaz et al., 2012; Gel'man et al., 1979; Jessup et al., 2015; Krasnopolsky, 2010b; Mahieux et al., 2023a; Marcq et al., 2008; Na et al., 1994; Oyama et al., 1980; Sandor et al., 2010) is decreased by a factor of 10, in line with below-cloud concentrations adopted by current photochemistry models (e.g., Krasnopolsky, 2012; Stolzenbach et al., 2023; Winick & Stewart, 1980).

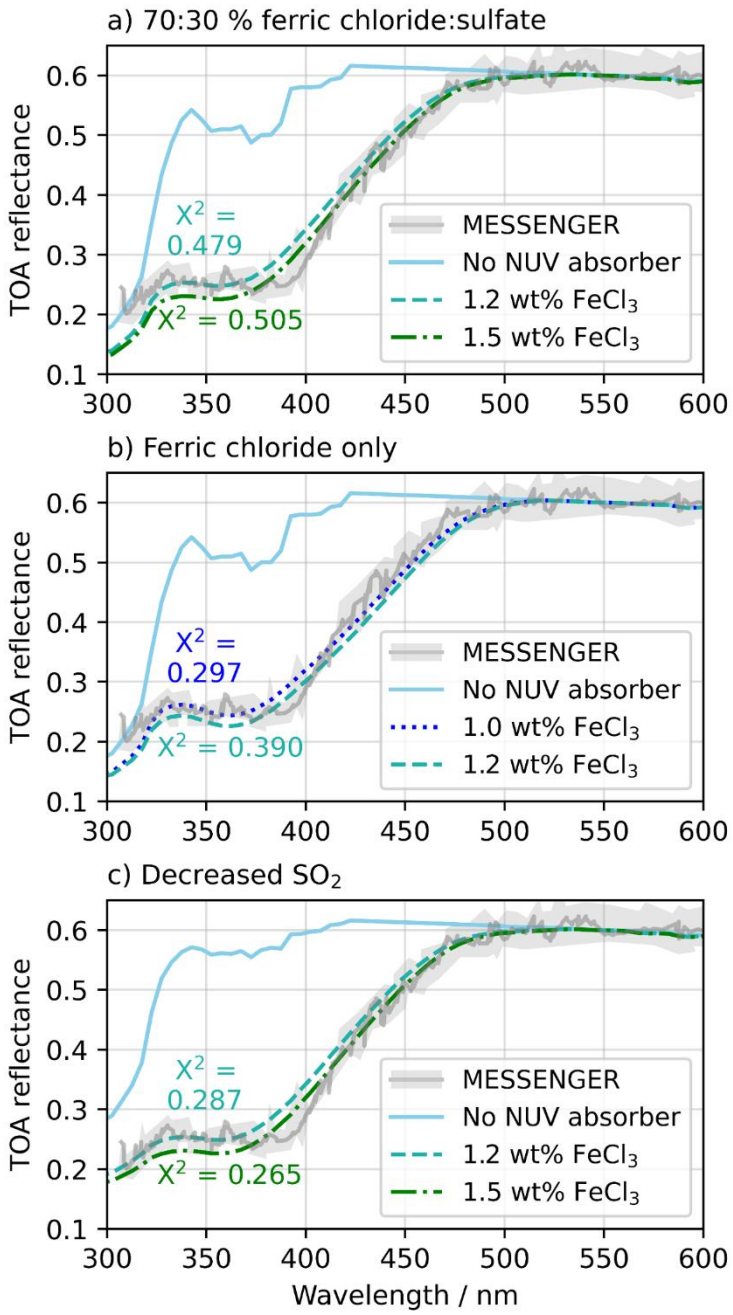

331

332 **Figure 5.** Modelled reflectance for varying initial concentrations of $FeCl_3$ in mode 1 using a) measured
333 spectra containing 70:30% ferric chloride:sulfate (Egan et al., 2025b), b) reconstructed spectra
334 containing only iron chloride contributions, or c) measured spectra as in a) but with the gas phase SO_2
335 mixing ratio decreased by a factor of 10 (light blue solid line). Different initial concentrations of $FeCl_3$
336 are compared to observations from MASCS/MESSENGER (grey line and uncertainty region, Pérez-
337 Hoyos et al., 2018). The quality of the fit is calculated as $X^2 = \sum_\lambda \left(\frac{observation-model}{observation}\right)^2$, where the
338 MESSENGER observations (grey line) have been interpolated to the wavelength (λ) values of the model.

The best fit results are for initial concentrations of 1.2 – 1.5 wt% $FeCl_3$ if ferric sulfate is formed (with improvement to the spectral shape from 300 – 350 nm if the atmospheric SO_2 is decreased), or 1.0 – 1.2 wt% $FeCl_3$ if the reaction to form sulfate is negligible in the upper clouds. The best fit $FeCl_3$ concentration in the absence of ferric sulfate is slightly higher than the equivalent $FeCl_3$ concentration in the 70:30 % $FeCl_3$:$Fe(SO_4)_2^-$ case due to the small contribution of ferric sulfate to the absorption at 300 – 400 nm. The refractive indices used for both cases are available in the SI (Table S6 and Figure S11).

4. Discussion

Examination of Figure 5 shows that the best fit initial concentration of $FeCl_3$ in mode 1 is 1.2 – 1.5 wt% $FeCl_3$ when partial conversion to ferric sulfate is assumed (resulting in an instantaneous concentration of approximately 0.85 – 1.0 wt% $FeCl_3$). The agreement of the measured spectrum (Figure 5a) with observations is excellent above 320 nm, and slightly too high below 320 nm, where the SO_2 contribution may be too high. Decreasing the gas-phase SO_2 by a factor of 10 throughout the atmosphere (Figure 5c), representing the possibility of historical errors in the measurement of SO_2 or wide variation in concentrations between measurements in different parts of the atmosphere (e.g., Belyaev et al., 2012; Jessup et al., 2015; Marcq et al., 2008; Sandor et al., 2010) improves the agreement of the spectral shape in this region. The removal of the ferric sulfate contribution similarly decreases the absorption below 320 nm – though the high SO_2 absorption is still dominant in this region – and the observed spectrum can be matched well with 1.0 – 1.2 wt% of $FeCl_3$. The minor difference in the $FeCl_3$ concentration providing the best fit for spectra containing ferric sulfate contributions and the best fit concentrations for pure ferric chloride spectra are likely due to a combination of uncertainty in the estimated concentrations of the measured spectra, and the contribution of the ferric sulfate to the absorption below 400 nm.

Assuming a purely meteoric source of vapourised Fe above the upper clouds, the required residence time of $FeCl_3$, τ_{FeCl_3}, in the upper cloud region (the only cloud region which the TOA reflectance model is sensitive to), can be estimated using Equation 6 (Section 2.3), with the height of injection of iron taken to be 100 km, the base of the injection profile; the column mass density of mode 1 particles above 60 km calculated to be 231 μg cm^{-2} from the V-PCM cloud model (Figure S6, SI); and the Fe mass input rate from meteoric ablation 4.2 ± 2.4 tonnes per Earth day (t d^{-1}) (Carrillo-Sánchez et al., 2020). If the formation of ferric sulfate is assumed to be negligible in the upper clouds and haze (i.e., the chemical lifetime of $FeCl_3$ in the upper clouds and haze exceeds the dynamical lifetime), ~1.1 wt% $FeCl_3$ in mode 1 would be sufficient to explain the absorption, requiring a residence time of 2800 years. If ferric sulfate formation cannot be neglected, an initial $FeCl_3$ concentration of ~1.4 wt% is required,

requiring 3400 years to accumulate sufficient iron. Additional loss processes of iron species, either chemical or dynamical, will require higher initial $FeCl_3$ concentrations, indicating either an additional source or a method of reforming $FeCl_3$ below the cloud top. The 58% uncertainty in the iron flux into the Venusian atmosphere (31 ± 18 t d^{-1}, approximately 13% of which ablates) introduces significant uncertainty in these values, as does the inability to run the chemical model to steady state due to the prohibitively long model run time that would be needed. While a residence time of several thousand years may seem high, we note that the reported iron bulk mass loading of 0.21 ± 0.06 mg m^{-3} in the cloud layer measured by the Venera 12 descender (Petryanov et al., 1981) is comparable to the total mode 1 mass loading in the upper clouds, and recent reanalysis of Pioneer Venus Large Probe descent data identified 1.1 ± 0.2 mg m^{-3} of $Fe_2(SO_4)_3$ (equivalent to 0.31 ± 0.06 mg m^{-3} Fe) in the lower cloud (Mogul et al., 2025). Iron mass loadings, and therefore residence times, significantly higher than required to account for only a small percentage of the mode 1 cloud particles are therefore clearly feasible in the Venusian clouds.

The altitude range over which the absorber is present is uncertain. Cloud top reflectance measurements, such as those used in this study, are not sensitive to the lower altitudes of the cloud deck, leaving the concentration of the absorber unconstrained in this region. Bertaux et al. (1996) reported that the ultraviolet spectrometers on Vega 1 and 2 descent probes returned absorption spectra they attribute to lower cloud particles, suggesting the UV absorber is present throughout the cloud deck. In this case, $FeCl_3$ could be present throughout the clouds deck in either mode 1 or multiple modes. This would require a greater iron column mass within the clouds, so a method of reforming $FeCl_3$ from $Fe_2(SO_4)_3$ in the lower clouds would be required. However, comparison of the visible and ultraviolet radiometers on the Pioneer Venus descent probes led Pollack et al. (1979) to tentatively conclude that visible absorption occurs only near the cloud tops. This may indicate the presence of more than one species contributing to the absorption at the cloud tops, or a change in composition through the cloud deck. Due to the limitations of the retrieval sensitivity in the lower clouds, we can draw no robust conclusions on this matter. However, a layer of $FeCl_3$ in the upper clouds above an iron sulphate reservoir (either $Fe_2(SO_4)_3$ or other forms (Jiang et al., 2024; Mogul et al., 2025)) in the lower clouds would be consistent with the Pioneer Venus radiometry and gas chromatograph reanalysis.

Previous work has also reported a good fit for 1 wt% $FeCl_3$ in sulfuric acid (Krasnopolsky, 2017; Zasova et al., 1981), though their reported best fit was for the mode 2 cloud droplets. While the model is sensitive to the mode 2 contribution, we found that higher concentrations (~10 wt%, Figure 4) were required in mode 2 to provide the observed absorption. While mode 1 was found to be the dominant contributor to the absorption, the precise concentrations in each mode that best reproduce the absorption will vary based on the precise treatment of cloud modes. The clouds adopted throughout

406 this work are constrained to the standard cloud model measured by the Pioneer Venus Large Probe
407 Cloud Particle Size Spectrometer (LCPS) (Knollenberg & Hunten, 1980), and particles are constrained
408 to the altitude bands of the different cloud layers. More recent studies (e.g. Luginin et al., 2024; Luginin
409 et al., 2016; Satoh et al., 2015; Wilquet et al., 2009) have reported both smaller and larger modal sizes
410 in the upper haze layer and upper clouds, indicating probable bimodality. The adoption of these
411 changes to the cloud model would be expected to subtly change the best fit concentrations in the
412 different cloud modes, though testing this hypothesis is beyond the scope of this study.

413 While mode 1 particles in the upper clouds are stable against sedimentation (Stolzenbach et al., 2023),
414 local variations in vertical winds will likely transport the particles throughout the atmosphere in less
415 than the timescale discussed above. Some recycling of ferric sulphate into NUV-absorbing species is
416 therefore expected: Jiang et al. (2024) reported that iron sulfate minerals can form from ferric chloride
417 in the cloud droplets, and absorb in the near-UV. If this occurs in the upper cloud layer, the reaction of
418 the $FeCl_3$ to form sulfate species would no longer be a sink with regard to the near-UV absorber.
419 Furthermore, any iron-containing cloud droplets that sediment to the bottom of the cloud deck will
420 evaporate (Titov et al., 2018), leaving residual nano-sized iron sulfate/oxide particles (Frankland et al.,
421 2017) which can then react with atmospheric HCl at elevated tropospheric temperatures below the
422 cloud base to reform $FeCl_3$ once again. Such small particles are not expected to be able to sediment
423 far in the high pressure conditions of the troposphere, but the reactions could occur either while in
424 the atmosphere or at the surface if sedimentation does occur. Reanalysis of measurements from the
425 Pioneer Venus Large Probe Neutral Mass Spectrometer detected 16 ± 3 wt% $Fe_2(SO_4)_3$ in the aerosols
426 of the lower clouds (Mogul et al., 2025), and chemical modelling of the lower haze region measured
427 by the Pioneer Venus Large Probe (Knollenberg & Hunten, 1980) predicted $FeCl_2$ and FeS_2 below the
428 main cloud deck (Woitke et al., 2025), both of which may provide an iron reservoir for the reformation
429 and recirculation of $FeCl_3$.

430 Transport and recycling of iron chloride can explain the large-scale inhomogeneities of the observed
431 absorption (Lee et al., 2015; Markiewicz et al., 2007; Titov et al., 2012; Titov et al., 2008), with regions
432 of higher or lower $FeCl_3$ concentration resulting from the upwelling of recycled material from the lower
433 clouds. The reaction of ferric chloride to ferric sulfate is expected to depend on temperature and HCl
434 concentration, and Jiang et al. (2024) found the formation of iron sulfate minerals depended strongly
435 on water availability, making the UV-brightness or -darkness of upwelled material dependent on the
436 local conditions in the atmosphere. The meteoric input provides a small but continuous source of fresh
437 $FeCl_3$ entering the clouds from above. In contrast, recycling of iron in the lower atmosphere would
438 produce an intermittent source of $FeCl_3$ from below the cloud top; upwelling of particles from a locally
439 warm or HCl-poor region of the atmosphere would produce a region of droplets with lower ferric

chloride concentration, while upwelling from a locally cold or HCl-rich part of the atmosphere would produce a region of droplets with higher ferric chloride concentration. As such, we would not expect a simple correlation of stronger absorption with either atmospheric upwelling or downwelling, as either may produce higher- or lower-concentration regions of $FeCl_3$.

Unlike for Mars and Earth (Carrillo-Sánchez et al., 2020; Crismani et al., 2017; Gómez Martín et al., 2017; Grebowsky et al., 2017; Plane, 2003a; 2018a; Plane et al., 2015), no reliable measurements of meteoric metal fluxes have been made in the Venusian atmosphere, so uncertainties in the meteoric input are large (31 ± 18 t d^{-1}) (Carrillo-Sánchez et al., 2020). Of the major meteoric metals, the atomic Na layer should be the most straightforward to observe in Venus's upper atmosphere because of the relatively high abundance of injected Na (Carrillo-Sánchez et al., 2020) and its strong optical transition at 589 nm (the terrestrial Na layer has been observed using both solar-pumped resonance fluorescence (Fan et al., 2007) and stellar occultation (Fussen et al., 2010)). The differential ablation of Fe to Na in Venus' atmosphere produces a relative elemental injection ratio of 4.5 (Carrillo-Sánchez et al., 2020), from which an estimate of the Fe layer abundance could be obtained (assuming similar rates of removal of both metals). Note that the relative Na to Fe flux produced by ablation in the Earth's upper atmosphere has been measured directly using co-located Na and Fe lidars(Huang et al., 2015); this data was then used to determine the relative contributions of cosmic dust particles from Jupiter Family Comets, the main asteroid belt, and Long Period Comets (Carrillo-Sánchez et al., 2016).

The 58% uncertainty on meteoric input means that the available iron flux may differ significantly from the values adopted in this work, thereby increasing or decreasing the required iron residence time. Measurements of meteoric metals in the Venusian atmosphere are therefore vitally important for constraining the achievable atmospheric $FeCl_3$ concentration and consequently its contribution to the NUV absorption.

5. Conclusions

We present radiative transfer modelling of Venus in the near-UV and visible wavelength range, including absorption by $FeCl_3$ measured in sulfuric acid (Egan et al., 2025b) in the different cloud modes. The best agreement of the shape and strength of the absorption predicted with the retrieved spectrum from the MASCS spectrometer on the MESSENGER spacecraft (Pérez-Hoyos et al., 2018) is for 1.0 – 1.2 wt% $FeCl_3$ in the mode 1 cloud droplets. The spectrum can also be reproduced by the inclusion of $FeCl_3$ in all cloud droplets, but mode 1 alone is the dominant contribution. The residence lifetime of iron in the clouds required for a purely meteoric source of iron to produce sufficient $FeCl_3$ to explain the absorption is probably between 2800 and 3400 years. The required concentration of iron in the upper clouds is lower than the observed iron mass loadings in the lower clouds (Mogul et

al., 2025; Petryanov et al., 1981), suggesting, in the absence of a known alternative source of iron into the clouds, that long residence times are expected in the cloud deck.

Reformation of $FeCl_3$ from other iron species in the clouds or deep atmosphere (Jiang et al., 2024; Mogul et al., 2025; Woitke et al., 2025) is likely required to increase the effective chemical lifetime of $FeCl_3$ or other absorber candidates to a scale comparable with the required residence time. Such reformation may explain the inhomogeneity of the observed absorption, with local variations in temperature, water availability, and HCl concentration changing the rate of formation and loss of $FeCl_3$, and producing regions of locally $FeCl_3$-rich or -poor droplets. Further work is required to explore these processes of conversion and/or reformation of $FeCl_3$ in the clouds and lower atmosphere. In the present study, we have presented a chemical scheme for the initial production of $FeCl_3$ from meteoric Fe atoms and atmospheric HCl and Cl, probably of volcanic origin. The chemical scheme has been implemented in the V-PCM PCM (e.g., Garate-Lopez & Lebonnois, 2018; Martinez et al., 2024; Martinez et al., 2023; Stolzenbach et al., 2023), and the dominant Fe species below 100 km was found to be $FeCl_3.CO_2$, which would be taken up into the cloud droplets as $FeCl_3$.

The excellent spectral agreement of the $FeCl_3$, the reasonable predicted concentrations of $FeCl_3$ compared to the observed iron mass loading, and the proposed mechanism for forming $FeCl_3$ above the clouds, make $FeCl_3$ the most promising candidate for the cause of the Venusian unknown UV absorption.

Acknowledgements

We thank the UK Science and Technology Research Council for funding this study (project ST/T000279/1). JVE acknowledges funding for a PhD studentship from the UK Engineering and Physical Sciences Research Council (EP/S023593/1). Aurélien Stolzenbach acknowledges the support of project PID2021-126365NB-C21 funded by the Agencia Estatal de Investigación (MCIN/AEI/10.13039/501100011033/) and FEDER.

We would also like to thank an anonymous reviewer for providing the simplified Kooij forms of reaction rates 5 and 9 in Table 1.

Conflicts of interest

The authors declare there are no conflicts of interest for this manuscript.

Open Research

Data to reproduce all figures in the main paper and Supplementary Information is available at Zenodo, via https://doi.org/10.5281/zenodo.17487186 (Egan, 2025).

The Venus Climate Database (2023) is available at http://www-venus.lmd.jussieu.fr/.

References

Ando, H., Imamura, T., Tellmann, S., Pätzold, M., Häusler, B., Sugimoto, N., et al. (2020). Thermal structure of the Venusian atmosphere from the sub-cloud region to the mesosphere as observed by radio occultation. *Scientific Reports, 10*(1), 3448. https://doi.org/10.1038/s41598-020-59278-8

Aoshima, H., Satoh, K., Umemura, T., & Kamigaito, M. (2013). A simple combination of higher-oxidation-state FeX_3 and phosphine or amine ligand for living radical polymerization of styrene, methacrylate, and acrylate. *Polymer Chemistry, 4*(12), 3554–3562. http://doi.org/10.1039/C3PY00352C

Belyaev, D. A., Montmessin, F., Bertaux, J.-L., Mahieux, A., Fedorova, A. A., Korablev, O. I., et al. (2012). Vertical profiling of SO_2 and SO above Venus' clouds by SPICAV/SOIR solar occultations. *Icarus, 217*(2), 740–751. https://doi.org/10.1016/j.icarus.2011.09.025

Bertaux, J.-L., Vandaele, A.-C., Korablev, O., Villard, E., Fedorova, A., Fussen, D., et al. (2007). A warm layer in Venus' cryosphere and high-altitude measurements of HF, HCl, H_2O and HDO. *Nature, 450*(7170), 646–649. https://doi.org/10.1038/nature05974

Bertaux, J.-L., Widemann, T., Hauchecorne, A., Moroz, V. I., & Ekonomov, A. P. (1996). VEGA 1 and VEGA 2 entry probes: An investigation of local UV absorption (220 – 400 nm) in the atmosphere of Venus (SO_2 aerosols, cloud structure). *Journal of Geophysical Research: Planets, 101*(E5), 12709–12745. https://doi.org/10.1029/96JE00466

Bézard, B., Bergh, C., Fegley, B., Maillard, J.-P., Crisp, D., Owen, T., et al. (1993). The abundance of sulfur dioxide below the clouds of Venus. *Geophysical Research Letters, 20*. https://doi.org/10.1029/93GL01338

Bézard, B., de Bergh, C., Crisp, D., & Maillard, J.-P. (1990). The deep atmosphere of Venus revealed by high-resolution nightside spectra. *Nature, 345*(6275), 508–511. https://doi.org/10.1038/345508a0

Bones, D. L., Daly, S. M., Mangan, T. P., & Plane, J. M. C. (2020). A study of the reactions of Ni^+ and NiO^+ ions relevant to planetary upper atmospheres. *Phys.Chem.Chem.Phys., 22*, 8940–8951. https://doi.org/10.1039/d0cp01124j

Bones, D. L., Plane, J. M. C., & Feng, W. (2016). Dissociative recombination of FeO^+ with electrons: implications for plasma layers in the ionosphere. *The Journal of Physical Chemistry A, 120*(9), 1369–1376. https://doi.org/10.1021/acs.jpca.5b04947

Carrillo-Sánchez, J. D., Gómez-Martín, J. C., Bones, D. L., Nesvorný, D., Pokorný, P., Benna, M., et al. (2020). Cosmic dust fluxes in the atmospheres of Earth, Mars, and Venus. *Icarus, 335*, 113395. doi.org/10.1016/j.icarus.2019.113395

Carrillo-Sánchez, J. D., Nesvorny, D., Pokorny, P., Janches, D., & Plane, J. M. C. (2016). Sources of cosmic dust in the Earth's atmosphere. *Geophys. Res. Lett., 43*(23), 11979–11986. Article. 10.1002/2016gl071697

Crismani, M. M. J., Schneider, N. M., Plane, J. M. C., Evans, J. S., Jain, S. K., Chaffin, M. S., et al. (2017). Detection of a persistent meteoric metal layer in the Martian atmosphere. *Nature Geoscience, 10*(6), 401–404. https://doi.org/10.1038/ngeo2958

Crisp, D. (1986). Radiative forcing of the Venus mesosphere: I. Solar fluxes and heating rates. *Icarus, 67*(3), 484–514. https://doi.org/10.1016/0019-1035(86)90126-0

Edwards, J. M., & Slingo, A. (1996). Studies with a flexible new radiation code. I: Choosing a configuration for a large-scale model. *Quarterly Journal of the Royal Meteorological Society, 122*(531), 689–719. https://doi.org/10.1002/qj.49712253107

Egan, J. V. (2025). *Ferric chloride: the Venusian unknown UV absorber?* [Dataset]. Zenodo - EU Open Research Repository. https://doi.org/10.5281/zenodo.20088448

Egan, J. V., Feng, W., James, A. D., Manners, J., Marsh, D. R., Lebonnois, S., et al. (2025a). Is OSSO a significant contributor to the unknown UV absorber in Venus' atmosphere? *Geophysical Research Letters, 52*(4), e2024GL113090. https://doi.org/10.1029/2024GL113090

555 Egan, J. V., James, A. D., & Plane, J. M. C. (2025b). Laboratory measurements of ferric chloride ($FeCl_3$)
556 under Venusian conditions. *ACS Earth and Space Chemistry*.
557 https://doi.org/10.1021/acsearthspacechem.5c00132
558 Encrenaz, T., Greathouse, T. K., Roe, H., Richter, M., Lacy, J., Bézard, B., et al. (2012). HDO and SO_2
559 thermal mapping on Venus: evidence for strong SO_2 variability. *Astronomy & Astrophysics,*
560 *543*, A153. https://doi.org/10.1051/0004-6361/201219419
561 Esposito, L. W., Knollenberg, R. G., Marov, M. Y., Toon, O. B., & Turco, R. P. (1983). The clouds and
562 hazes of Venus. In *Venus* (pp. 484).
563 Eymet, V., Fournier, R., Dufresne, J.-L., Lebonnois, S., Hourdin, F., & Bullock, M. A. (2009). Net
564 exchange parameterization of thermal infrared radiative transfer in Venus' atmosphere.
565 *Journal of Geophysical Research: Planets, 114*(E11). https://doi.org/10.1029/2008JE003276
566 Fan, Z. Y., Plane, J. M. C., Gumbel, J., Stegman, J., & Llewellyn, E. J. (2007). Satellite measurements of
567 the global mesospheric sodium layer. *Atmos. Chem. Phys., 7*, 4107–4115.
568 https://doi.org/10.5194/acp-7-4107-2007
569 Feng, W., Marsh, D. R., Chipperfield, M. P., Janches, D., Hoeffner, J., Yi, F., & Plane, J. M. C. (2013). A
570 global atmospheric model of meteoric iron. *Journal of Geophysical Research: Atmospheres,*
571 *118*(16), 9456–9474. https://doi.org/10.1002/jgrd.50708
572 Francés-Monerris, A., Carmona-García, J., Trabelsi, T., Saiz-Lopez, A., Lyons, J. R., Francisco, J. S., &
573 Roca-Sanjuán, D. (2022). Photochemical and thermochemical pathways to S_2 and polysulfur
574 formation in the atmosphere of Venus. *Nature Communications, 13*(1), art. no.: 4425.
575 https://doi.org/10.1038/s41467-022-32170-x
576 Frankland, V. L., James, A. D., Carrillo-Sánchez, J. D., Nesvorný, D., Pokorný, P., & Plane, J. M. C. (2017).
577 CO oxidation and O_2 removal on meteoric material in Venus' atmosphere. *Icarus, 296*, 150–
578 162. https://doi.org/10.1016/j.icarus.2017.06.005
579 Frisch, M. J., Trucks, G. W., Schlegel, H. B., Scuseria, G. E., Robb, M. A., Cheeseman, J. R., et al. (2016).
580 Gaussian 16 Rev. C.01. Wallingford, CT: Gaussian Inc. Retrieved from
581 https://gaussian.com/gaussian16/
582 Fussen, D., Vanhellemont, F., Tetard, C., Mateshvili, N., Dekemper, E., Loodts, N., et al. (2010). A
583 global climatology of the mesospheric sodium layer from GOMOS data during the 2002-2008
584 period. *Atmos. Chem. Phys., 10*(19), 9225–9236. https://doi.org/10.5194/acp-10-9225-2010
585 Gao, P., Zhang, X., Crisp, D., Bardeen, C. G., & Yung, Y. L. (2014). Bimodal distribution of sulfuric acid
586 aerosols in the upper haze of Venus. *Icarus, 231*, 83–98.
587 https://doi.org/10.1016/j.icarus.2013.10.013
588 Garate-Lopez, I., & Lebonnois, S. (2018). Latitudinal variation of clouds' structure responsible for
589 Venus' cold collar. *Icarus, 314*, 1–11. https://doi.org/10.1016/j.icarus.2018.05.011
590 Gel'man, B. G., Zolotukhin, V. G., Lamonivm, N. I., Levchuk, B. V., Mukhin, L. M., Nenarokov, D. F., et
591 al. (1979). *Analiz khimicheskogo sostava atmosfery venery na AMS Venera-12 gazovym*
592 *khromatografom*. Retrieved from https://ntrs.nasa.gov/citations/19790017793
593 Georgievskii, Y., & Klippenstein, S. J. (2005). Long-range transition state theory. *Journal of Chemical*
594 *Physics, 122*, art. no. 194103. https://doi.org/10.1063/1.1899603
595 Giesen, A., Herzler, J., & Roth, P. (2002). High temperature oxidation of iron atoms by CO_2. *Physical*
596 *Chemistry Chemical Physics, 4*, 3665–3668. https://doi.org/10.1039/B201822E
597 Gilbert, R. G., & Smith, S. C. (1990). *Theory of unimolecular and recombination reactions*. Oxford:
598 Blackwell.
599 Gilli, G., Navarro, T., Lebonnois, S., Quirino, D., Silva, V., Stolzenbach, A., et al. (2021). Venus upper
600 atmosphere revealed by a GCM: II. Model validation with temperature and density
601 measurements. *Icarus, 366*, 114432. https://doi.org/10.1016/j.icarus.2021.114432
602 Glowacki, D. R., Liang, C.-H., Morley, C., Pilling, M. J., & Robertson, S. H. (2012). MESMER: An open-
603 source Master Equation Solver for Multi-Energy well Reactions. *The Journal of Physical*
604 *Chemistry A, 116*(38), 9545–9560. https://doi.org/10.1021/jp3051033

Gómez-Martín, J. C., Seaton, C., Miranda, M. P. d., & Plane, J. M. C. (2017). The Reaction between Sodium Hydroxide and Atomic Hydrogen in Atmospheric and Flame Chemistry. *J. Phys. Chem. A, 121*, 7667–7674. https://doi.org/10.1021/acs.jpca.7b07808

Gómez Martín, J. C., Brooke, J. S. A., Feng, W., Höpfner, M., Mills, M. J., & Plane, J. M. C. (2017). Impacts of meteoric sulfur in the Earth's atmosphere. *Journal of Geophysical Research: Atmospheres, 122*(14), 7678–7701. https://doi.org/10.1002/2017JD027218

Goody, R., West, R., Chen, L., & Crisp, D. (1989). The correlated-k method for radiation calculations in nonhomogeneous atmospheres. *Journal of Quantitative Spectroscopy and Radiative Transfer, 42*(6), 539–550. https://doi.org/10.1016/0022-4073(89)90044-7

Gordon, I. E., Rothman, L. S., Hargreaves, R. J., Hashemi, R., Karlovets, E. V., Skinner, F. M., et al. (2022). The HITRAN2020 molecular spectroscopic database. *Journal of Quantitative Spectroscopy and Radiative Transfer, 277*, 107949. https://doi.org/10.1016/j.jqsrt.2021.107949

Grebowsky, J. M., Benna, M., Plane, J. M. C., Collinson, G. A., Mahaffy, P. R., & Jakosky, B. M. (2017). Unique, non-Earthlike, meteoritic ion behavior in upper atmosphere of Mars. *Geophysical Research Letters, 44*(7), 3066–3072. https://doi.org/10.1002/2017GL072635

Hapke, B., & Graham, F. (1989). Spectral properties of condensed phases of disulfur monoxide, polysulfur oxide, and irradiated sulfur. *Icarus, 79*(1), 47–55. https://doi.org/10.1016/0019-1035(89)90107-3

Helmer, M., & Plane, J. M. C. (1994). Kinetic study of the reaction between Fe and O_3 under mesospheric conditions. *Journal of the Chemical Society, Faraday Transactions, 90*, 31–37 https://doi.org/10.1039/FT9949000031

Huang, W., Chu, X., Gardner, C. S., Carrillo-Sánchez, J. D., Feng, W., Plane, J. M. C., & Nesvorný, D. (2015). Measurements of the vertical fluxes of atomic Fe and Na at the mesopause: Implications for the velocity of cosmic dust entering the atmosphere. *Geophys. Res. Lett.*, 2014GL062390. https://doi.org/10.1002/2014GL062390

Janches, D., Swarnalingam, N., Carrillo-Sanchez, J. D., Gomez-Martin, J. C., Marshall, R., Nesvorný, D., et al. (2017). Radar Detectability Studies of Slow and Small Zodiacal Dust Cloud Particles. III. The Role of Sodium and the Head Echo Size on the Probability of Detection. *Astrophys. J., 843*, art. no. 1. https://doi.org/10.3847/1538-4357/aa775c

Jessup, K. L., Marcq, E., Mills, F., Mahieux, A., Limaye, S., Wilson, C., et al. (2015). Coordinated Hubble Space Telescope and Venus Express observations of Venus' upper cloud deck. *Icarus, 258*, 309–336. https://doi.org/10.1016/j.icarus.2015.05.027

Jiang, C. Z., Rimmer, P. B., Lozano, G. G., Tosca, N. J., Kufner, C. L., Sasselov, D. D., & Thompson, S. J. (2024). Iron-sulfur chemistry can explain the ultraviolet absorber in the clouds of Venus. *Science Advances, 10*(1), eadg8826. https://doi.org/10.1126/sciadv.adg8826

Karyu, H., Kuroda, T., Imamura, T., Terada, N., Vandaele, A. C., Mahieux, A., & Viscardy, S. (2024). One-dimensional Microphysics Model of Venusian Clouds from 40 to 100 km: Impact of the Middle-atmosphere Eddy Transport and SOIR Temperature Profile on the Cloud Structure. *The Planetary Science Journal, 5*(3), 57. https://doi.org/10.3847/PSJ/ad25f3

Karyu, H., Kuroda, T., Määttänen, A., Mahieux, A., Viscardy, S., Terada, N., et al. (2026). A cosmic origin of Venus' lower haze. *Nature Astronomy, 10*(7), 964–971. https://doi.org/10.1038/s41550-026-02843-4

Knollenberg, R. G., & Hunten, D. M. (1979). Clouds of Venus: a preliminary assessment of microstructure. *Science, 205*(4401), 70–74. https://doi.org/10.1126/science.205.4401.70

Knollenberg, R. G., & Hunten, D. M. (1980). The microphysics of the clouds of Venus: results of the Pioneer Venus Particle Size Spectrometer experiment. *Journal of Geophysical Research: Space Physics, 85*(A13), 8039–8058. https://doi.org/10.1029/JA085iA13p08039

Krasnopolsky, V. A. (2010a). Spatially-resolved high-resolution spectroscopy of Venus 1. Variations of CO_2, CO, HF, and HCl at the cloud tops. *Icarus, 208*(2), 539–547. https://doi.org/10.1016/j.icarus.2010.02.012

Krasnopolsky, V. A. (2010b). Spatially-resolved high-resolution spectroscopy of Venus 2. Variations of HDO, OCS, and SO_2 at the cloud tops. *Icarus, 209*(2), 314–322. https://doi.org/10.1016/j.icarus.2010.05.008

Krasnopolsky, V. A. (2012). A photochemical model for the Venus atmosphere at 47–112km. *Icarus, 218*(1), 230–246. https://doi.org/10.1016/j.icarus.2011.11.012

Krasnopolsky, V. A. (2017). On the iron chloride aerosol in the clouds of Venus. *Icarus, 286*, 134–137. https://doi.org/10.1016/j.icarus.2016.10.003

Kuiper, G. P. (1969). The identification of the Venus cloud layers. *Communications of the Lunar and Planetary Laboratory, 6*, 229–248. Retrieved from https://ntrs.nasa.gov/citations/19700004516

Lee, Y. J., Imamura, T., Schröder, S. E., & Marcq, E. (2015). Long-term variations of the UV contrast on Venus observed by the Venus Monitoring Camera on board Venus Express. *Icarus, 253*, 1–15. https://doi.org/10.1016/j.icarus.2015.02.015

Lee, Y. J., Muñoz, A. G., Yamazaki, A., Quémerais, E., Mottola, S., Hellmich, S., et al. (2022). Reflectivity of Venus's dayside disk during the 2020 observation campaign: outcomes and future perspectives. *The Planetary Science Journal, 3*(9), 209. https://doi.org/10.3847/PSJ/ac84d1

Lefèvre, M., Lefèvre, F., Määttänen, A., Skog, R., Frandsen, B., Stolzenbach, A., & Braude, A. (2026). The Impact of the Sulfur Allotropes and Sulfur Hydrides on the Venus Cloud Chemistry. *Journal of Geophysical Research: Planets, 131*(5), e2025JE009523. https://doi.org/10.1029/2025JE009523

Liu, W., Etschmann, B., Brugger, J., Spiccia, L., Foran, G., & McInnes, B. (2006). UV–Vis spectrophotometric and XAFS studies of ferric chloride complexes in hyper-saline LiCl solutions at 25–90 °C. *Chemical Geology, 231*(4), 326–349. https://doi.org/10.1016/j.chemgeo.2006.02.005

Luginin, M., Fedorova, A., Belyaev, D., Montmessin, F., Korablev, O., & Bertaux, J. L. (2024). Bimodal aerosol distribution in Venus' upper haze from joint SPICAV-UV and -IR observations on Venus Express. *Icarus, 409*, 115866. https://doi.org/10.1016/j.icarus.2023.115866

Luginin, M., Fedorova, A., Belyaev, D., Montmessin, F., Wilquet, V., Korablev, O., et al. (2016). Aerosol properties in the upper haze of Venus from SPICAV IR data. *Icarus, 277*, 154–170. https://doi.org/10.1016/j.icarus.2016.05.008

Mahieux, A., Robert, S., Mills, F. P., Jessup, K. L., Trompet, L., Aoki, S., et al. (2023a). Update on SO_2, detection of OCS, CS, CS_2, and SO_3, and upper limits of H_2S and HOCl in the Venus mesosphere using SOIR on board Venus Express. *Icarus, 399*, 115556. https://doi.org/10.1016/j.icarus.2023.115556

Mahieux, A., Robert, S., Piccialli, A., Trompet, L., & Vandaele, A. C. (2023b). The SOIR/Venus Express species concentration and temperature database: CO_2, CO, H_2O, HDO, $H^{35}Cl$, $H^{37}Cl$, HF individual and mean profiles. *Icarus, 405*, 115713. https://doi.org/10.1016/j.icarus.2023.115713

Mangan, T. P., Harman-Thomas, J. M., Lade, R. E., Douglas, K. M., & Plane, J. M. C. (2020). Kinetic study of the reactions of AlO and OAlO relevant to planetary mesospheres. *ACS Earth Space Chem., 4*, 2007–2017. https://doi.org/10.1021/acsearthspacechem.0c00197

Manners, J., Edwards, J. M., Hill, P., & Thelen, J.-C. (2022a). *SOCRATES technical guide*. Retrieved from https://code.metoffice.gov.uk/trac/socrates

Manners, J., Edwards, J. M., Hill, P., & Thelen, J.-C. (2022b). *SOCRATES user guide*. Retrieved from https://code.metoffice.gov.uk/trac/socrates

Marcq, E., Bézard, B., Drossart, P., Piccioni, G., Reess, J. M., & Henry, F. (2008). A latitudinal survey of CO, OCS, H_2O, and SO_2 in the lower atmosphere of Venus: spectroscopic studies using VIRTIS-H. *Journal of Geophysical Research: Planets, 113*(E5). https://doi.org/10.1029/2008JE003074

Markiewicz, W. J., Titov, D. V., Limaye, S. S., Keller, H. U., Ignatiev, N., Jaumann, R., et al. (2007). Morphology and dynamics of the upper cloud layer of Venus. *Nature, 450*(7170), 633–636. https://doi.org/10.1038/nature06320

Martinez, A., Chaufray, J.-Y., Lebonnois, S., Gonzàlez-Galindo, F., Lefèvre, F., & Gilli, G. (2024). Three-dimensional Venusian ionosphere model. *Icarus, 415*, 116035. https://doi.org/10.1016/j.icarus.2024.116035

Martinez, A., Lebonnois, S., Millour, E., Pierron, T., Moisan, E., Gilli, G., & Lefèvre, F. (2023). Exploring the variability of the venusian thermosphere with the IPSL Venus GCM. *Icarus, 389*, 115272. https://doi.org/10.1016/j.icarus.2022.115272

Mogul, R., Zolotov, M. Y., Way, M. J., & Limaye, S. S. (2025). Re-Analysis of Pioneer Venus Data: Water, Iron Sulfate, and Sulfuric Acid are Major Components in Venus' Aerosols. *Journal of Geophysical Research: Planets, 130*(9), e2024JE008582. https://doi.org/10.1029/2024JE008582

Montgomery, J. A., Frisch, M. J., Ochterski, J. W., & Petersson, G. A. (2000). A complete basis set model chemistry. VII. Use of the minimum population localization method. *The Journal of Chemical Physics, 112*, 6532–6542. https://doi.org/10.1063/1.481224

Na, C. Y., Esposito, L. W., McClintock, W. E., & Barth, C. A. (1994). Sulfur dioxide in the atmosphere of Venus: II. modeling results. *Icarus, 112*(2), 389–395. https://doi.org/10.1006/icar.1994.1193

Nahar, S. N., Bautista, M. A., & Pradhan, A. K. (1997). Electron-ion recombination of neutral iron. *The Astrophysical Journal, 479*(1), 497–503. https://doi.org/10.1086/303874

Oyama, V. I., Carle, G. C., Woeller, F., Pollack, J. B., Reynolds, R. T., & Craig, R. A. (1980). Pioneer Venus gas chromatography of the lower atmosphere of Venus. *Journal of Geophysical Research: Space Physics, 85*(A13), 7891–7902. https://doi.org/10.1029/JA085iA13p07891

Palmer, K. F., & Williams, D. (1975). Optical constants of sulfuric acid; application to the clouds of Venus? *Applied Optics, 14*(1), 208–219. https://doi.org/10.1364/AO.14.000208

Pérez-Hoyos, S., Sánchez-Lavega, A., García-Muñoz, A., Irwin, P. G. J., Peralta, J., Holsclaw, G., et al. (2018). Venus upper clouds and the UV absorber from MESSENGER/MASCS observations. *Journal of Geophysical Research: Planets, 123*(1), 145–162. https://doi.org/10.1002/2017JE005406

Petryanov, I. V., Andreichikov, B. M., Korchuganov, B. N., Ovsyankin, E. I., Ogorodnikov, B. I., Skitovich, V. I., & Khristianov, V. K. (1981). Iron in Venus clouds. *Dokl. Akad. Naik. SSP, 206*, 834–836. Retrieved from http://mi.mathnet.ru/eng/dan/v260/i4/p834

Pinto, J. P., Li, J., Mills, F. P., Marcq, E., Evdokimova, D., Belyaev, D., & Yung, Y. L. (2021). Sulfur monoxide dimer chemistry as a possible source of polysulfur in the upper atmosphere of Venus. *Nature Communications, 12*(1), 175. https://doi.org/10.1038/s41467-020-20451-2

Plane, J. M. C. (2003a). Atmospheric chemistry of meteoric metals. *Chemical Reviews, 103*(12), 4963–4984. https://doi.org/10.1021/cr0205309

Plane, J. M. C. (2003b). Atmospheric chemistry of meteoric metals. *Chem. Rev., 103*(12), 4963–4984. 10.1021/cr0205309

Plane, J. M. C., Carrillo-Sanchez, J. D., Mangan, T. P., Crismani, M. M. J., Schneider, N. M., & Määttänen, A. (2018a). Meteoric metal chemistry in the Martian atmosphere. *Journal of Geophysical Research: Planets, 123*(3), 695–707. https://doi.org/10.1002/2017JE005510

Plane, J. M. C., Carrillo-Sanchez, J. D., Mangan, T. P., Crismani, M. M. J., Schneider, N. M., & Määttänen, A. (2018b). Meteoric Metal Chemistry in the Martian Atmosphere. *J. Geophys. Res.-Planets, 123*, 695–707. 10.1002/2017JE005510

Plane, J. M. C., Feng, W., & Dawkins, E. C. M. (2015). The mesosphere and metals: chemistry and changes. *Chemical Reviews, 115*(10), 4497–4541. https://doi.org/10.1021/cr500501m

Pollack, J. B., Ragent, B., Boese, R., Tomasko, M. G., Blamont, J., Knollenberg, R. G., et al. (1979). Nature of the ultraviolet absorber in the Venus clouds: inferences based on Pioneer Venus data. *Science, 205*(4401), 76–79. https://doi.org/10.1126/science.205.4401.76

Rollason, R. J., & Plane, J. M. C. (1998). A study of the reactions of Fe^+ with O_3 , O_2 and N_2. *Journal of the Chemical Society, Faraday Transactions, 94*, 3067–3075. https://doi.org/10.1039/A805140B

Rollason, R. J., & Plane, J. M. C. (2000). The reactions of FeO with O_3, H_2, H_2O, O_2 and CO_2. *Physical Chemistry Chemical Physics, 2*(10), 2335–2343. https://doi.org/10.1039/B000877J

Ross, F. E. (1928). Photographs of Venus. *The Astrophysical Journal, 68*, 57. https://doi.org/10.1086/143130

Rossow, W. B., Del Genio, A. D., Limaye, S. S., Travis, L. D., & Stone, P. H. (1980). Cloud morphology and motions from Pioneer Venus images. *Journal of Geophysical Research: Space Physics, 85*(A13), 8107–8128. https://doi.org/10.1029/JA085iA13p08107

Rutherford, J. A., & Vroom, D. A. (1972). Formation of iron ions by charge transfer. *The Journal of Chemical Physics, 57*, 3091–3093. https://doi.org/10.1063/1.1678724

Sandor, B. J., Todd Clancy, R., Moriarty-Schieven, G., & Mills, F. P. (2010). Sulfur chemistry in the Venus mesosphere from SO_2 and SO microwave spectra. *Icarus, 208*(1), 49–60. https://doi.org/10.1016/j.icarus.2010.02.013

Satoh, T., Ohtsuki, S., Iwagami, N., Ueno, M., Uemizu, K., Suzuki, M., et al. (2015). Venus' clouds as inferred from the phase curves acquired by IR1 and IR2 on board Akatsuki. *Icarus, 248*, 213–220. https://doi.org/10.1016/j.icarus.2014.10.030

Scalmani, G., Frisch, M. J., Mennucci, B., Tomasi, J., Cammi, R., & Barone, V. (2006). Geometries and properties of excited states in the gas phase and in solution: theory and application of a time-dependent density functional theory polarizable continuum model. *The Journal of Chemical Physics, 124*, 094107. https://doi.org/10.1063/1.2173258

Seiff, A., Schofield, J. T., Kliore, A. J., Taylor, F. W., Limaye, S. S., Revercomb, H. E., et al. (1985). Models of the structure of the atmosphere of Venus from the surface to 100 kilometers altitude. *Advances in Space Research, 5*(11), 3–58. https://doi.org/10.1016/0273-1177(85)90197-8

Self, D. E., & Plane, J. M. C. (2003). A kinetic study of the reactions of iron oxides and hydroxides relevant to the chemistry of iron in the upper mesosphere. *Physical Chemistry Chemical Physics, 5*(7), 1407–1418. https://doi.org/10.1039/b211900e

Skog, R., Frandsen, B., & Kurtén, T. (2024). *Simulating UV-Vis spectra for polysulfur species in the Venusian atmosphere*. Paper presented at the EGU General Assembly 2024, Vienna, Austria.

Smirnov, V. N. (2008). Rate constant of the gas-phase reaction between Fe atoms and CO_2. *Kinetics and Catalysis, 49*, 607–609. https://doi.org/10.1134/S0023158408050017

Smith, I. W. M. (1980). *Kinetics and dynamics of elementary gas reactions*. London: Butterworths.

Stolzenbach, A., Lefèvre, F., Lebonnois, S., & Määttänen, A. (2023). Three-dimensional modeling of Venus photochemistry and clouds. *Icarus, 395*, 115447. https://doi.org/10.1016/j.icarus.2023.115447

Tellmann, S., Pätzold, M., Häusler, B., Bird, M. K., & Tyler, G. L. (2009). Structure of the Venus neutral atmosphere as observed by the radio science experiment VeRa on Venus Express. *Journal of Geophysical Research: Planets, 114*(E9). https://doi.org/10.1029/2008JE003204

Titov, D. V., Ignatiev, N. I., McGouldrick, K., Wilquet, V., & Wilson, C. F. (2018). Clouds and hazes of Venus. *Space Science Reviews, 214*(8), 126. https://doi.org/10.1007/s11214-018-0552-z

Titov, D. V., Markiewicz, W. J., Ignatiev, N. I., Song, L., Limaye, S. S., Sanchez-Lavega, A., et al. (2012). Morphology of the cloud tops as observed by the Venus Express Monitoring Camera. *Icarus, 217*(2), 682–701. https://doi.org/10.1016/j.icarus.2011.06.020

Titov, D. V., Taylor, F. W., Svedhem, H., Ignatiev, N. I., Markiewicz, W. J., Piccioni, G., & Drossart, P. (2008). Atmospheric structure and dynamics as the cause of ultraviolet markings in the clouds of Venus. *Nature, 456*(7222), 620–623. https://doi.org/10.1038/nature07466

Tobiska, W. K., Woods, T., Eparvier, F., Viereck, R., Floyd, L., Bouwer, D., et al. (2000). The SOLAR2000 empirical solar irradiance model and forecast tool. *Journal of Atmospheric and Solar-Terrestrial Physics, 62*(14), 1233–1250. https://doi.org/10.1016/S1364-6826(00)00070-5

Tomasko, M. G., Smith, P. H., Suomi, V. E., Sromovsky, L. A., Revercomb, H. E., Taylor, F. W., et al. (1980). The thermal balance of Venus in light of the Pioneer Venus Mission. *Journal of Geophysical Research: Space Physics, 85*(A13), 8187–8199. https://doi.org/10.1029/JA085iA13p08187

Vandaele, A. C., De Mazière, M., Drummond, R., Mahieux, A., Neefs, E., Wilquet, V., et al. (2008). Composition of the Venus mesosphere measured by solar occultation at infrared on board Venus Express. *Journal of Geophysical Research: Planets, 113*(E5). https://doi.org/10.1029/2008JE003140

Vandaele, A. C., Korablev, O., Belyaev, D., Chamberlain, S., Evdokimova, D., Encrenaz, T., et al. (2017). Sulfur dioxide in the Venus atmosphere: I. Vertical distribution and variability. *Icarus, 295*, 16–33. https://doi.org/10.1016/j.icarus.2017.05.003

Venus Climate Database. (2023). The Venus Climate Database v2.3 [Dataset]. Retrieved from http://www-venus.lmd.jussieu.fr/

Vondrak, T., Woodcock, K. R. I., & Plane, J. M. C. (2006). A kinetic study of the reactions of Fe^+ with N_2O, N_2, O_2, CO_2 and H_2O, and the ligand-switching reactions $Fe^+.X + Y \rightarrow Fe^+.Y + X$ (X = N_2, O_2, CO_2; Y=O_2, H_2O). *Physical Chemistry Chemical Physics, 8*(4), 503–512. https://doi.org/10.1039/b508922k

Whalley, C. L., & Plane, J. M. C. (2010). Meteoric ion layers in the Martian atmosphere. *Faraday Disc., 147*, 349–368. https://doi.org/10.1039/c003726e

Williams, L. R., & Golden, D. M. (1993). Solubility of HCl in sulfuric acid at stratospheric temperatures. *Geophysical Research Letters, 20*(20), 2227–2230. https://doi.org/10.1029/93GL02607

Wilquet, V., Drummond, R., Mahieux, A., Robert, S., Vandaele, A. C., & Bertaux, J.-L. (2012). Optical extinction due to aerosols in the upper haze of Venus: Four years of SOIR/VEX observations from 2006 to 2010. *Icarus, 217*(2), 875–881. https://doi.org/10.1016/j.icarus.2011.11.002

Wilquet, V., Fedorova, A., Montmessin, F., Drummond, R., Mahieux, A., Vandaele, A. C., et al. (2009). Preliminary characterization of the upper haze by SPICAV/SOIR solar occultation in UV to mid-IR onboard Venus Express. *Journal of Geophysical Research: Planets, 114*(E9). https://doi.org/10.1029/2008JE003186

Winick, J. R., & Stewart, A. I. F. (1980). Photochemistry of SO2 in Venus' upper cloud layers. *Journal of Geophysical Research: Space Physics, 85*(A13), 7849–7860. https://doi.org/10.1029/JA085iA13p07849

Woitke, P., Scherf, M., Helling, C., Rimmer, P., Ferus, M., Lammer, H., et al. (2025). Prediction of Sulfate Hazes in the Lower Venus Atmosphere. *The Planetary Science Journal, 6*(9), 225. https://doi.org/10.3847/PSJ/ae00bf

Woodcock, K. R. S., Vondrak, T., Meech, S. R., & Plane, J. M. C. (2006). A kinetic study of the reactions FeO^++O, $Fe^+.N_2$ + O, $Fe^+.O_2$ + O and FeO^+ + CO: implications for sporadic E layers in the upper atmosphere. *Physical Chemistry Chemical Physics, 8*(15), 1812–1821. https://doi.org/10.1039/B518155K

Wright, W. H. (1927). Photographs of Venus made by infra-red and by violet light. *Publications of the Astronomical Society of the Pacific, 39*(230), 220–221. https://doi.org/10.1086/123718

Young, L. D. G. (1972). High resolution spectra of Venus—a review. *Icarus, 17*(3), 632–658. https://doi.org/10.1016/0019-1035(72)90029-2

Zasova, L. V., Krasnopolsky, V. A., & Moroz, V. I. (1981). Vertical distribution of SO_2 in upper cloud layer of Venus and origin of U.V.-absorption. *Advances in Space Research, 1*(9), 13–16. https://doi.org/10.1016/0273-1177(81)90213-1